Toward high-energy-density lithium metal batteries: opportunities and challenges for solid organic electrolytes

Towards high energy density lithium metal batteries: opportunities and challenges for solid organic electrolytes

Xiaoen Wang,[*] Robert Kerr, Fangfang Chen, Nicolas Goujon,

*Jennifer M. Pringle, David Mecerreyes, Maria Forsyth, Patrick C. Howlett **

Dr. X. Wang, Dr. R. Kerr, Dr. F. Chen, Dr. N. Goujon, Dr. J. M. Pringle, Prof. M. Forsyth, Prof. P. C. Howlett
Institute for Frontier Materials (IFM)
Deakin University
Geelong, VIC 3217, Australia.
E-mail: xiaoen.wang@deakin.edu.au; patrick.howlett@deakin.edu.au

Dr. F. Chen, Dr. J. M. Pringle, Prof. M. Forsyth, Prof. P. C. Howlett
ARC Centre of Excellence for Electromaterials Science (ACES)
Deakin University,
Burwood, VIC 3125, Australia

Dr. Nicolas Goujon, Prof. D. Mecerreyes, Prof. M. Forsyth
POLYMAT University of the Basque Country UPV/EHU
Joxe Mari Korta Center, Avda. Tolosa72, 20018 Donostia-San Sebastian, Spain

Keywords

organic ionic plastic crystals, polymer electrolytes, high energy density, lithium metal, solid-state lithium batteries

Abstract

With increasing demands for safe, high capacity energy storage to support personal electronics, newer devices such as unmanned aerial vehicles, as well as the commercialization of electric vehicles (EVs), current energy storage technologies are facing increased challenges. Although alternative batteries have been intensively investigated, lithium (Li) batteries are still recognized as the preferred energy storage solution for consumer electronics markets and next generation automobiles. However, the commercialized Li batteries still have disadvantages such as low capacities, potential safety issues and unfavorable cycling life. Therefore, the design and development of electromaterials towards high energy density, long life-span Li batteries with improved safety is a focus for researchers in the field of energy materials. Herein, recent advances in the development of novel organic electrolytes are summarized towards solid-state Li batteries (SSLBs) with higher energy density and improved safety. On the basis of new insights into ionic conduction and design principles of organic based solid-state electrolytes (SSEs), specific strategies towards developing these electrolytes for Li metal anodes, high energy density cathode materials (e.g. high voltage materials) as well as the optimization of cathode formulations are outlined. Finally, prospects for next generation solid-state electrolytes are also proposed.

1. Introduction

The ever-growing consumer electronic market such as portable electronics, wearable devices and the commercialization of electric vehicles (EVs) have greatly motivated the pursuit of efficient, safe batteries that can be used for long service times. Although great efforts have been made to develop other alternative batteries, such as using Na, K or Mg as anodes,[1] they are still nascent compared with Li batteries. Li metal is known for its extremely high theoretical specific capacity (c.a. 3860 mAh g^{-1}) due to its low density (0.53 g cm^{-3}) and ultra-negative electrochemical potential (-3.04 V vs. standard hydrogen electrode, SHE). However, this intrinsic high capacity has not yet been achieved due to its high reactivity and the potential safety concerns such as battery fire, explosion etc. Therefore, the design of high energy density Li-based batteries with improved safety is critically important for next generation batteries and applications.

For electrochemical energy storage devices, the energy density, or specific energy of a Li battery is defined as the energy stored per unit volume (Wh L^{-1}) or per unit mass (Wh kg^{-1}), which is related to the intrinsic capacity and properties of the cathode, anode and, of course, the whole integrated battery device.[2] For cathode materials, high energy density can be achieved either by using high capacity active materials or by increasing the operating voltage. From the materials design point of view, increasing the operating voltage of the cathode can be achieved, for example, by transition metal ion substitution or doping based on the existing systems.[3, 4] Achieving a new high capacity cathode normally requires the invention of new compounds, usually at the expense of achieving high voltage, thus limiting the increase in overall energy density. As an example, after Ni substitution, the energy density of $LiNi_{0.5}Mn_{1.5}O_4$ can reach up to 650 Wh kg^{-1} with a discharge plateau around 4.7 V, which is 1.6 times higher than the energy of spinel $LiMn_2O_4$ (400 Wh kg^{-1}). [4, 5] However, the use of high voltage

cathodes is limited by the properties of the electrolyte materials, such as chemical/electrochemical stability. Since the commercialization of the first generation Li batteries was demonstrated by Sony in the 1990s,[6] organic solvent-based liquid electrolytes such as ethylene carbonate (EC) and dimethyl carbonate (DMC) have conventionally been used. These organic liquid electrolytes provide high room temperature conductivity and suitable electrochemical stability towards most of the electrode systems such as $LiFePO_4$ (LFP) or $LiCoO_2$ (LCO). Unfortunately, they are highly flammable and volatile, and also show unsatisfactory stability against high voltage cathode materials (e.g. >4.5 V). Thus, safety concerns (e.g. fire, explosion) become a significant issue when the batteries are heated due to high-current charge/discharge or when short circuits occur due to Li dendrite formation. Therefore, the development of high energy Li batteries requires safe and efficient electrolyte systems, and while high voltage cathode systems were proposed nearly 40 years ago, the current commercialized battery systems are yet to safely realise their potential.

The development of electrolyte systems with high safety is crucial for achieving safe and high energy batteries. Over the decades, several systems have been proposed and intensively investigated in terms of improving Li battery safety. For instance, aqueous electrolytes are the recently emerging family of safe electrolytes. However, due to the low electrochemical stability of H_2O, these electrolytes are highly limiting to the cell voltage, which also restricts the improvement of capacity compared with conventional Li batteries. Although there are breakthroughs such as “water-in-salt” electrolytes that have been reported recently,[7] the energy density of aqueous battery materials is still not comparative to the state-of-the-art of high voltage batteries. Inorganic solid-state electrolytes (SSEs) represent another family of promising materials for SSLBs. The first report of inorganic electrolyte assembled batteries dates back to as early as the

1960s, when β-alumina ($Na_2O \cdot 11Al_2O_3$) was demonstrated as a solid electrolyte in high temperature sodium-sulfur batteries.[8] Benefiting from the unique structure and ion dynamics, inorganic SSEs provide very high ionic conductivity (10^{-3} S cm^{-1} at room temperature), high Li^+ transference number (t_{Li+}, close to 1) as well as a wide electrochemical stability window. However, these electrolytes are rigid and create poor solid-solid interface contact between the electrode and electrolyte, leading to significantly high interfacial resistance.[9] Other drawbacks such as poor chemical stability can be found in some representative systems such as LiPON, NASICON and $Li_7P_3S_{11}$ electrolytes,[10] in which the reduction reaction between inorganic electrolytes and Li metal anode inevitably form unstable interfacial SEI layers.[11] It should also be pointed out that, in practical applications, it is a challenge to completely remove the pores in inorganic electrolyte pellets (usually higher than 5% [12]), under which conditions the Li dendrites can still penetrate the electrolyte and short-circuit the cells.

In summary, current SSEs still show problems such as poor interface stability especially when paired with high voltage cathode materials, [13] limited kinetics in high loading electrodes, high electrode/electrolyte interfacial resistance, and unfavorable mechanical stability/integrity for large-scale battery applications. Thus, in the pursuit of high energy Li metal batteries, the main strategies will include how to design compatible electrolyte materials and how to correspondingly formulate the cathode composition to improve electrode/electrolyte charge transfer and enhance active material loading. Commercially, the demonstration of polyethylene oxide (PEO) based Li metal polymer batteries (30 kWh packs, 100Wh kg^{-1} at 70-80 ˚C) by Bollore Blue Solutions for diverse applications including as car-sharing EVs, shows that these barriers can be overcome.[14] Meanwhile, higher rate performance, higher energy density and ambient temperature operation remain as goals for researchers and industry alike to further the development

of SSLBs. In order to address the above challenges, this review will focus on our recent advances and strategies which particularly focus on the state-of-the art of the emerging organic based SSEs (e.g. organic plastic crystals, alternative polymer electrolytes and composite systems). These soft materials are often at the limit between solid electrolytes and ionic liquids, encompassing many of their benefits but also addressing solid-state electrolyte issues of interfacial stability and contact as well as processability. Furthermore, combined with computational simulations, the principles and strategies for future electrolyte systems with improved Li^+ transport are proposed.

2. Organic ionic plastic crystals (OIPCs) as solid-state electrolytes

2.1. OIPCs and their phase-dependent behaviors

Organic ionic plastic crystals (OIPCs) represent a class of SSE consisting of small organic molecular ions. Compared with molecular plastic crystals such as succinonitrile,[15] OIPCs are considered as safe electrolytes due to their ionic nature resulting in non-volatility and negligible vapor pressure even after melting. Thus, OIPCs have been extensively investigated and used in a range of devices, such as proton exchange membrane fuel cells,[16] dye-sensitized solar cells,[17] capacitors[18] and next generation high energy batteries (e.g. Li-, Na- batteries).[19] There are several reviews that have summarized the classification and basic physical chemical properties of OIPCs,[20, 21, 22] which are not the focus of this section. Instead, here we will discuss their ionic conductivity and its dependence on phase behavior, then more focus will be given to understanding ion transport in different OIPC-based composites in terms of their applications in SSLBs. One of the key properties of OIPCs that has driven research interest is related to their enhanced interfacial stability and ability to form stable, low resistance interphases at electrodes after charge-discharge cycling. This so-called 'pre-conditioning effect' has been shown to be due the OIPCs ability to modify it's transport

properties and microstructure at the electrode interface.[19, 23] This aspect is still being explored along with the role of additional interfaces created during the formation of composite materials, discussed in more detail in later sections.

(Figure 1)

OIPCs have been proposed as one of the promising electrolyte materials due to favorable plasticity, which can greatly improve the solid/solid contact for SSLBs. The ion conduction of OIPCs is highly dependent on their phase behavior. Thus, the understanding of the relationship between phase behaviors and ion transport is critically important for the design of high performance OIPC-based electrolytes. **Figure 1**a shows the ion pair structure of a typical OIPC diethyl(methyl)(isobutyl)phosphonium hexafluorophosphate, $[P_{122i4}][PF_6]$.[24] In the low temperature phase (phase IV), both the cations and anions are highly ordered with a crystal structure of orthorhombic *Pbca* group. As stated in previous literature,[22] the phase I is defined as the highest temperature phase below melting, and the subsequent phases at lower temperatures are denoted as phases II, III, IV, etc. Within each solid phase, the ionic conductivity continuously increases with increasing temperature, while it often jumps to a much higher value at the onset of a solid-solid phase transition (Figure 1b). For instance, in low temperature ordered phase IV, the ionic conductivity is below 10^{-9} S cm^{-1}, then the conductivity significantly increases to 10^{-4} and 10^{-3} S cm^{-1} in highly disordered phase II and phase I, respectively. This evolution of the ionic conductivity is highly related with the motional modes of cations, anions (Figure 1c) and their relationship to defect formation (e.g. vacancies) during structural rearrangement. The doping of salt (e.g. Li^+ or Na^+) can further increase the concentrations of defects in the electrolytes, resulting in significantly increased conductivity.[25] For example, the 10 mol% Li salt doped pyrrolidinium-based OIPCs (e.g. $[C_2mpyr][FSI]$ and $[C_2mpyr][FSI]$) can show

conductivity enhancements of more than two orders of magnitude compared with the bulk material.[26, 27] However, due to the formation of more disordered phases or the presence of highly mobile phases, the enhanced ionic conductivity is unfortunately often followed by the deterioration of mechanical properties (i.e. they become too soft to be used as free-standing electrolytes), which hinders their large-scale applications due to the raised concern of dendrite formation in the case where Li metal is used. To address this issue, we have developed OIPC-based composite materials by using nanoparticles and nanofibers. This section presents the recent advances of OIPC-based composite electrolyte design in terms of Li metal battery applications, and how the interfacial behavior between OIPC and polymer surfaces affects the ion dynamics and transport.

2.2. Second phase effects in OIPC composite electrolytes

Although OIPCs have demonstrated respectable properties in terms of the ionic conductivity and good electrochemical stability (e.g. 5.6 V vs Li^+/Li [28]), several aspects still need to be further improved for future battery applications. For example, some OIPCs with "rigid" anions (e.g. BF_4, PF_6) normally show high thermal stability which can keep their solid-state at high temperature up to 200 °C, however the low temperature conductivity is not suitable for battery applications. Other systems with more flexible anions (e.g. TFSI, FSI) show high ionic conductivity at room temperature, while they are too soft to be used as free-standing electrolytes. For instance, the OIPC triisobutyl methylphosphonium bis(fluorosulfonyl)imide ($[P_{1i4i4i4}][FSI]$) has a melting point around 37 °C; although the conductivity can be enhanced at least four orders of magnitude at room temperature after Li salt doping, an additional polyethylene separator is needed for battery assembly.[29] For the application of these OIPC-based electrolytes in practical devices, our strategy is to develop OIPC-based composite

electrolytes by incorporation of a second, structural component, and to understand the effects of this second component on composite electrolyte properties such as ion dynamics, mechanical properties and, ultimately, practical device performance.

2.2.1 Effects of inorganic nanoparticles

Adebahr *et al* reported the first OIPC-composite by including nano size TiO_2 particles in the OIPC [C_2mpyr][TFSI], *N*-ethyl-*N*-methyl pyrrolidinium bis(trifluoromethane sulfonyl)amide. The conductivity of [C_2mpyr][TFSI] composites with 10 wt% of TiO_2 increased by more than one order of magnitude.[30] In another report, when SiO_2 nanoparticles were incorporated within the same OIPC, an even more significant conductivity enhancement was observed, and it was concluded that the addition of SiO_2 can effectively increase the mobile defects, subsequently increasing the plasticity and the ion dynamics.[31] However, the conductivity enhancement via nanoparticle incorporation is not applicable to all the OIPC systems. Pringle *et al* compared the effects of different nanoparticles on the phase behaviors and conductivity of a range of OIPCs. [32] The conductivity measurements showed that the significant enhancement is usually observed in less plastic phases with low conductivity. For the OIPCs intrinsically containing a high concentration of defects, the addition of nanoparticles did not lead to conductivity enhancement and could even decrease the conductivity. This observation is similar to another report by Shekibi *et al*. [33] When SiO_2 was added into Li salt doped [C_2mpyr][TFSI], the overall conductivity of the composite decreased significantly, which is in contrast to either Li salt doping or SiO_2 nanoparticle addition to pure [C_2mpyr][TFSI]. The exact mechanisms of conductivity changes in these systems is still unclear, but it is apparent that transport mechanisms change as a result of forming the OIPC-based inorganic nanoparticle composites.

2.2.2. Effects of polymer nano fillers

In addition to inorganic nanoparticles, OIPC composites with polymer nanofibers or nanoparticles were also developed, and some of the systems have been successfully used in Li metal batteries. Compared with the nanoparticle composites, the use of nanofibers can significantly improve flexibility of the electrolyte membranes. Howlett *et al* first demonstrated an OIPC composite consisting of $LiBF_4$ doped $[C_2mpyr][BF_4]$ and PVDF electrospun fibers.[34] Benefiting from the flexible support of PVDF fibers, the mechanical properties were greatly improved, resulting in a thin and flexible composite SSE. Encouragingly, the prepared composites showed improved conductivity at moderate temperatures which enabled LFP full cell cycling at 50 °C. Iranipour *et al* investigated the effects of PVDF nanofibers on the phase transition and ion dynamics.[35] Interestingly, in contrast to other reported OIPC systems which show enhanced conductivity after Li salt doping, the conductivity of 10 mol% $LiBF_4$ doped $[C_2mpyr][BF_4]$ only showed enhanced conductivity in phase I while a decreased conductivity was observed in the lower temperature phase II. Further studies including DSC, powder diffraction and solid-state NMR revealed that the Li salt doping resulted in the formation of a second, Li-rich phase which limits the ion dynamics in the lower temperature phase. At higher temperatures (phase I), this second phase is removed and a higher conductivity relative to the pure OIPC is achieved. Analysis of the PVDF composites showed that the secondary Li-rich phase was absent, leading to enhanced conductivity in phase II and highlighting the effect of polymer nanofibers on phase behavior and ion dynamics in OIPC materials.

We can further speculate that this conductivity change is likely related to the interface region between the OIPC and polymer surfaces as evidenced by the dependence of conductivity on different polymer chemistries (**Figure 2**a, b). Particularly, the OIPC

composite incorporated with the poly(ionic liquid)s fiber, 10Li-[C_2mpyr][BF_4]/PDADMA TFSI, shows the highest conductivity in all composites. The Li | Li symmetric cell tests also confirm the superior electrochemical performance (low overpotential) of the PDADMA TFSI composite electrolyte (Figure 2c).

(Figure 2)

Another benefit of the fiber composite is that the polymer nanofibers can provide good mechanical integrity for these solid electrolytes. For example, the neat [C_2mpyr][FSI] shows high thermal stability and a wide plastic temperature range,[37] while the Li salt addition significantly decreases the mechanical strength of the electrolyte. By incorporation of PVDF fibers into this material, a free-standing OIPC composite electrolyte can be easily prepared even when 50 mol% Li salt is mixed with the [C_2mpyr][FSI]. As a result, the composite electrolyte, 50Li-[C_2mpyr][FSI]/PVDF, shows an electrochemical stability window up to 5.6 V and a t_{Li+} of 0.37.[28] The assembled solid-state Li | NMC111 cell demonstrates a promising capacity retention of 71% after 50 cycles (initial specific capacity 120 mAh g^{-1} vs 86 mAh g^{-1} at 50 cycles) at high cut-off voltage of 4.6 V, ambient temperature (Figure 2d).

While the polymer fibers have shown promising aspects in enhancing both electrochemical properties and mechanical properties of OIPC electrolytes, it is still a challenge to understand the mechanism of polymer surface effects due to the complicated geometry of fibrous supports. To overcome this, we have developed composite electrolytes with PVDF nanoparticles with controlled particle size and systematically varying composition, thereby investigating the effect of the interfacial region on the composite properties (**Figure 3**a). In contrast to the observation of inorganic nanocomposites discussed earlier, the PVDF nanoparticles showed an

increase in conductivity even in plastic phase I.[38] Figure 3b shows the comparison of conductivity as a function of nanoparticle loading, presenting a strong dependence on PVDF mass fraction and a higher conductivity in the 10 mol% LiFSI-doped OIPC composite at loadings above 30 wt% (the percolation value). This observation highlights that, in this particular composite, the PVDF nanoparticles can enhance the conductivity even in the presence of LiFSI salt, which is different from the $LiBF_4$-doped [C_2mpyr][BF_4] composites.[35] The enhancement in ion dynamics was also confirmed by static NMR measurements (^{7}Li NMR spectra, Figure 3c), with line narrowing observed in the composite. This again confirms the role of interfacial effects on ion dynamics and also demonstrates another strategy to enhance conductivity and to improve mechanical stability by using less expensive PVDF particles. In this case, the optimized electrolyte also demonstrated stable Li symmetric cycling performance as well as a stable, long-term Li | LFP full cell cycling at 2C and room temperature (Figure 3d).[39]

(Figure 3)

Following the same strategy, a high concentration LiFSI (50 mol% LiFSI/[C_2mpyr][FSI]) containing PVDF nanoparticles was proposed. In this case, increasing the Li salt concentration enabled a Li metal solid-state device with a high voltage NMC cathode (up to 4.6 V) (shown later in Figure 12a & b). The enhanced high voltage stability is attributed to the formation of a stable cathode/electrolyte interphase, as suggested by Wang et al.[40] Although these OIPC-based composites incorporating a nanostructured polymer component have shown promising battery performance, the exact mechanism of conductivity enhancement is still under investigation and further comparisons with inorganic nanocomposites and other polymer chemistries should be performed in the future.

Li^+ transference number is another important parameter to evaluate OIPC-based electrolytes. For the [C_2mpyr][FSI]-based electrolytes with different LIFSI concentrations, the PVDF fiber composite electrolytes containing 10 mol% LiFSI (10Li-[C_2mpyr][FSI]/PVDF fiber composite), 50 mol% LIFSI (50Li-[C_2mpyr][FSI]/PVDF fiber composite) show transference numbers of 0.1 and 0.37 at 50 °C, respectively. [27, 28] Interestingly, when PVDF nanoparticles were used, the 50Li-[C_2mpyr][FSI]/PVDF nanoparticle composite shows a transference number of 0.44, which is higher than the PVDF fiber composite containing the same LiFSI doped OIPC.[39] It should be noted that due to the different sample preparation method, nanoparticle composites contain higher loading of PVDF particles (60 wt%) than the fiber composites (10-15 wt%), suggesting higher specific contact area between PVDF and OIPCs. Therefore, we assume that the enhancement of the transference numbers could come from the surface interaction which depresses the FSI anion mobilities.

3. Ionic polymer-based solid-state electrolytes

Solid polymer electrolytes (SPEs) have shown their advantages in design of high energy density and all-solid-state batteries due to their flexibility and mechanical integrity.[41] In addition, due to the absence of organic carbonate plasticizers, the application of SPEs can greatly improve the battery safety, which is the key for large scale applications especially when Li metal is considered.

Since the first polymer electrolyte systems were developed by Michel Armand in the 1970s,[42] PEO and its derivatives have been extensively investigated as the mainstream system for polymer electrolytes.[43] PEO has a good ability to solvate Li^+ and dissociate Li salts. On the other hand, coordination between the PEO backbone and Li^+ ions is relatively strong, which in turn limits the mobility of the Li^+ ions. Therefore, although

PEO-based electrolytes have been largely used in different alternative battery devices such as the Blue Solutions vehicles discussed above, the t_{Li+} is still low (0.2~0.3) and new chemistries are desirable. Anionic polymer electrolytes have anions chemically bound to polymer side chains, and ideally the Li cation is the only mobile species, thus producing a single-ion conductor with a t_{Li+} of 1. However, the main disadvantage of these anionic polymers is the low ionic conductivity, due to the strong coulombic interaction between alkali cations and polyanions, leading to the virtual crosslinking of polymer chains that increases polymer T_g. Given the fact that T_g corresponds to the onset of segmental motions within the polymer backbone and, for most current polymer electrolyte systems, the ion mobility is highly correlated with these segmental motions, the T_g is an important parameter for the design of highly conductive polymer electrolytes.[44] A number of strategies have been tried to increase the alkali cation transport through modifying the polymer architectures, such as making block copolymers with ion-diffusion facilitating units (e.g. EO);[45] or adding ionic liquids /solvents as plasticizer. Different strategies have been developed in order to increase the Li^+ conductivity, all of which have an important role for the polymer.

3.1. Polycarbonate polymer electrolytes

Nowadays, other polymers such as polycarbonates (PCs) systems are being extensively investigated as alternatives to PEO due to their higher t_{Li+}.[44] The weak Li^+ coordination by carbonate groups and strong coordination with anions are considered to be the main reason for the observed values of t_{Li+} higher than 0.5 for PCs.[46, 47] At higher salt concentrations, the coordinated Li ions act as transient crosslinks that stiffen the material and hinder ion transport. However, employing 'plasticising anions' (e.g., LiTFSI) can achieve fast Li-ion conduction at high-salt concentrations although this is

accompanied by deterioration of the mechanical properties.[48] As an example, a series of poly(ethylene oxide carbonates) (PEO/PCs) were synthesized by polycondensation between different ethylene oxide diols and dimethyl carbonate. These PEO/PC systems were formulated as SPEs by adding different amounts of LiTFSI.[49] The concentratiom of LiTFSI was varied within the polymer resulting in a t_{Li+} of 0.59 and the highest ionic conductivity of 1.3×10^{-3} S cm^{-1} at 70 °C. Interestingly, at the same temperature, the electrochemical stability window was 4.9 V for these PEO/PCs SPEs.

A number of different single-ion conducting polymer electrolytes have been developed in recent years, as reviewed by Armand *et al.*[50] As an example, an optimized single-ion polymer electrolyte was recently synthesized by combining the most successful chemical units with respect to polymer electrolyte design, such as ethylene oxide, carbonate and Li sulfonimide.[51] The single-ion conducting PEO/PC copolymers showed high ionic conductivities of 1.2×10^{-4} S.cm^{-1} at 70 °C and t_{Li+}>0.89. The single-ion PEO/PC was compared with an analogous conventional polymer electrolyte containing an equivalent amount of LiTFSI salt. As expected, the ionic conductivity of the conventional salt in polymer electrolyte was higher. However, the effective Li^+ conductivity obtained by multiplying the total conductivity by the t_{Li+} of each system showed a more similar value of 2.9×10^{-5} S cm^{-1} for the single-ion PEO/PC compared with the conventional SPE PEO/PC with dual cation/anion motion, where the Li^+ conductivity was 7.9×10^{-5} S cm^{-1}. The performances of both polymer electrolytes in Li symmetric cells were compared (**Figure 4**). Interestingly, the single-ion polymer electrolyte showed improved performance in Li plating and stripping (lower cell voltage polarization), while both systems were able to sustain the applied current density. The single-ion system shows lower overpotential (80 mV *vs*. 180 mV) and a distinct plateau at 0.2 mA cm^{-2} (70 ºC), indicating that this system exhibits better Li^+

transport properties, while the conventional PEO/PC suffers from Li^+ transport limitations (Figure 4). The difference in Li^+ transport performance between the two systems is likely due to the presence of mobile TFSI anions in the conventional system, which reduces the fraction of charge carried by Li^+. This is reflected in the symmetrical cell polarisation profiles where the formation of a concentration gradient is evident from the absence of a sustained plateau in the potential profile of the cell with the conventional PEO-PC electrolyte.[52] The continuously increasing cell potential suggests a diffusion limited reaction at one or both electrodes, which is made worse by the mobility of TFSI in the conventional system, allowing it to more effectively crowd the interface.

(Figure 4)

3.2. Alternative polymers for high salt concentration polymer electrolytes

3.2.2. Poly(ionic liquid)s as polymer hosts

As noted above, due to the strong coordination between PEO oxygen and Li^+, the t_{Li+} in conventional PEO-based electrolytes is generally low (0.2~0.3). This is undesirable as it can result in high polarization and affects the charge-discharge performances, especially at high C-rate. To enhance the t_{Li+}, researchers have successfully developed a range of alternative polymer hosts that go beyond PEO and its derivatives, including the PC systems described above. [44]

It has been demonstrated that increasing the Li salt concentration, or using a solvent-in-salt system, can effectively increase the Li^+ transport.[7, 53] The mechanism lies in a dramatically changed coordination structure, in which ion hopping occurs via coordination exchange within extended aggregates wherein there are higher Li^+ -anion coordination numbers. This leads to a high t_{Li+}, although the conductivity is

decreased.[54] Ionic liquid (IL)-based electrolytes containing high salt content have also been investigated; their high safety characteristics and enhanced Li metal cycling making them alternative candidates for safe Li metal devices. Compared with electrolytes containing low LiFSI content (e.g. 0.8 mol kg^{-1}), increasing the LiFSI salt in pyrrolidinium-based FSI ionic liquids (e.g. 3.2 mol kg^{-1} or 1:1 mole ratio of IL to LiFSI salt) was shown to double the t_{Li+}, which enabled improved charge-discharge performance at high C-rate.[55]

High salt content strategies have also been used in polymer electrolyte systems.[56] In our recent work, we demonstrated that a poly(ionic liquid) (or polyIL) host can be a promising polymer matrix to dissolve high amounts of Li salt, resulting in high rate Li metal cycling, as well as full cells with high voltage cathodes such as NMC and NCA. In particular, we developed polymer electrolytes based on a low cost and commercially available polyIL, poly-(diallyldimethylammonium) (PDADMA) (**Figure 5**). This ionic polymer was selected as a result of its commercial availability, low cost as well the feasibility to simply tailor its chemistry by exchanging different counter ions. When the PDADMA TFSI was mixed with high LiFSI-containing phosphonium ionic liquids, an optimized ionic conductivity of 0.28 mS cm^{-1} was achieved at 30 ºC (Figure 5g). Although the t_{Li+} as measured by electrochemical methods (0.18 at 50 ºC) is lower than for the high LiFSI ionic liquids (0.59 at 50 ºC), the prepared electrolytes (Figure 5d) can still sustain long-term Li symmetric cycling at a high current density of 0.5 mA cm^{-2} (Figure 5d, f). It should also be noted that although diffusion NMR shows that the diffusion coefficient of all ionic charge carriers decreases with increased polyIL, the decrease of anion diffusion is more significant. In other words, this NMR result indicates the added polyIL enhances the Li^+ diffusion relative to other charged species, which is consistent with an earlier report by Schönhoff *et al.*[57] Furthermore, revisiting

the strategy of increasing target ion transport by nanoparticle addition discussed for OIPCs above (section 2), the addition of Al_2O_3 nanoparticles improves the mechanical stability. However, this mechanical enhancement from nanoparticle fillers is limited due to relatively weak interactions or entanglements between polymer and particle surfaces. To further investigate the effects of salt concentration on the properties of polyIL-based composite electrolytes and their electrochemistry, we developed PVDF nanofiber-enhanced composite polymer electrolytes, which allows control of the salt concentration over a wider range without loss of mechanical properties (Figure 5e). As shown in Figure 5h, the conductivity is highly dependent on the salt concentration; with increasing salt content from 1.6 mol kg^{-1} to 4.7 mol kg^{-1}, the conductivities decrease significantly from 4.5×10^{-4} to 4.9×10^{-6} S cm^{-1} at room temperature, while the t_{Li+} dramatically increases from 0.13 to 0.53. When the PVDF fibers were used as a reinforcement, the polyIL-based composite electrolytes with LiFSI content of 3.1 mol kg^{-1} demonstrated both high mechanical strength and stable Li metal cycling. This composite polymer electrolyte also supported stable charge-discharge full cell cycling with high loadings of both NMC and NCA cathodes, having an areal capacity of higher than 1 mAh cm^{-2}.

(Figure 5)

The composite polymer electrolyte investigations demonstrated that the polyILs have a critical role as polymer hosts and can themselves influence the Li^+ transport, which we attribute to specific interactions between the polymer and the salt anions affecting the ion transport mechanism. This electrostatic interaction or coordination was also mentioned by Smyrl *et al.* in their earlier work when PDADMA TFSI was used with tetraglyme (G4)-LiTFSI solvate ionic liquid.[61] To confirm this interaction in polyIL-based electrolytes, we have simplified the polymer electrolyte composition, by using

PDADMA FSI and LiFSI binary solid electrolytes (**Figure 6**a) and eliminating the ionic liquid component.[62] Interestingly, the addition of LiFSI salt continuously decreases the glass transition temperature (T_g) while the conventional PEO-based electrolytes show an increase T_g when salt concentrations is higher than 5 mol%.[63] In addition, the polyILs show good solubility towards high Li salt content and a homogenous phase is sustained up to 1:1.5 mole ratio of polyIL units to Li^+, where the highest ion conductivity is achieved (e.g. 1.1×10^{-5} S cm^{-1} at 50 °C) compared with other polyIL units to Li^+ ratios (**Figure 6**b). Assisted by molecular dynamics simulations, discussed in more detail below, it was confirmed that anions coordinate with both the polycation backbone ions and the Li^+, which synergistically immobilizes the anions and facilitates Li^+ transport. This co-coordination mechanism provides an alternative method to designing next generation polymer electrolytes with high t_{Li+} (> 0.5, **Figure 6**c). The best electrolytes in this family of materials show promising Li | Li symmetric cycling up to 0.2 mAh cm^{-2} and supported a Li | NMC full cell areal capacity of 1.1 mAh cm^{-2} at elevated temperature, as shown in **Figure 6**d.

(Figure 6)

As a summary, the polyILs have shown promising properties such as high Li salt solubility, wide electrochemical stability window and high thermal stability for future all solid state, safe batteries applications. However, the state-of-the-art polyILs still show low ambient conductivity and most of the demonstrations are based on plasticized systems, which unfortunately weakens their advantages as solid state electrolytes. Therefore, the improvement of room temperature conductivity along with balanced mechanical stability for polyIL platforms is a key goal for the design of high performance polymer electrolytes.

3.2.3. PolyIL block copolymer electrolytes

From the work described thus far, it is clear that the incorporation of high Li salt concentration in homopolymer-based polymer electrolytes comes at the cost of the mechanical properties. Furthermore, in some cases, especially for low temperature applications, small molecular plasticizers (e.g. ionic liquids,[65] carbonates[66]) are still needed in order to enhance the ionic conductivity, which consequently further deteriorates the mechanical stability and may lead to additional unwanted side reactions within the electrodes during device operation. To overcome this plasticizing effect, the use of a polyIL block copolymer, where a high T_g polymer block is covalently bonded to the ionic conducting block, was recently proposed as the polymer host for Li salts.[67] Herein, a polystyrene (PS) block was used as a mechanical block to overcome the plasticizing effect of ionic liquid and LiFSI (**Figure 7**a), which were selectively solubilized in the polyIL blocks. Furthermore, the DSC and integrated SAXS patterns (Figure 7b-c) suggest that a microphase separation (ionic liquid, LiFSI salt rich phase and PS rich phase) with lamellar structure is maintained. By this strategy, the mechanical and ion-conduction properties can be tuned independently by precisely controlling the degree of polymerization of each block using RAFT techniques. It was found that a molar ratio of 4:1 between the mechanical block and the polyILs block, respectively, gave the best compromise in terms of mechanical and ion conduction properties. Additionally, the use of polyIL block allows the dissolution of Li salt at much higher concentration when compared to ionic liquid alone, as seen in PDAMDA based systems discussed above. The development of SPEs with enhanced Li^+ transport properties (t_{Li}≈ 0.5) was achieved by keeping the overall anion to Li molar ratio below a value of 1.5, through the use of high Li salt concentration.[67] These SPE materials demonstrated promising performance in a Li metal battery with a LFP cathode at 50 °C

(Figure 7d), near practical operating levels (1.8 $mAh.cm^{-2}$) without the need for additional reinforcement. These materials provide a vast selection of chemistries to tailor both conductivity, Li^+ transport and mechanical properties by control of block length, block chemistry and salt concentration. We are currently investigating these parameters in order to further improve the electrolyte performance for SSLBs operating with high capacity cathodes.

(Figure 7)

3.3. Alternative Li salt design

The enhanced Li^+ transport properties observed in superconcentrated electrolytes has been attributed to the formation of multi-dentate anion-Li^+-coordination in order to satisfy the Li^+ coordination environment. With increasing lithium salt content, the average number of anions coordinating with one Li^+ (coordination number) progressively decreased (i.e., on average each anion coordinates with more than one Li^+, which is indicative of ion clustering or aggregates. [62][68] The formation of such aggregates results in a change of the transport mechanism present in these materials, shifting from a typical vehicular transport mechanism to a Li^+ hopping-like transport mechanism,[69] similar to the Grotthus transport mechanism in acid media.

Following this concept of promoting anion interactions to enhance Li^+ transport properties, Armand *et al.* recently developed novel TFSI-like anions with hydrogen bond donor groups for solid-state Li metal batteries. [70, 71] The replacement of some fraction of the F atoms in the TFSI anion by a hydrogen atom allows additional hydrogen interaction between the anions themselves and also the polymer host, which results in an enhancement of the Li^+ conductivity (Figure 8). These new anions have thus far only been investigated in PEO based SPEs, providing great scope for additional

studies in other polymer matrices as well in gel and polyIL systems such as those described here. As the TFSI and FSI anions facilitated a step change in the electrolyte evolution after 1990 (both liquid and polymer electrolytes) due to their plasticizing properties and unique ability to form stable SEI layers on electrode surfaces,[72] so these new anions will promote an entirely new family of electrolyte materials with still higher Li^+ transport relative to the present systems.

(Figure 8)

4. Simulation-assisted design of new solid-state electrolytes

Concurrent with experimental studies, computational research has demonstrated its power in exploring new electrolyte materials, rational design and optimization of existing electrolyte systems, through expanding fundamental knowledge at the molecular level and assisting the interpretation of experimental observations.[73]. The current computational methods used in electrolyte research are normally divided into first-principle based methods [e.g. *ab initio*, Density Functional Theory (DFT)], classical force field based methods [e.g. Monte Carlo (MC), Molecular dynamics (MD)], and their combination, ab initio molecular dynamics (AIMD) method. First-principle methods are generally used to study ion-ion interactions and their structures. They are also widely used to interpret experimental spectroscopy properties, including Infrared (IR), Raman, and Nuclear Magnetic Resonance (NMR) spectroscopy etc. Due to the higher level calculation, their applications are limited to small molecular systems. Classical force field based methods, e.g. MD, are more often applied to investigate large electrolyte systems such as polymers. The MD method allows calculation of time-dependent properties, for instance, ion diffusion, which are very important in electrolyte research especially in disclosing relationships between ion coordination environments

and diffusion mechanisms. The AIMD method treats ion-ion interactions based on first-principles, and dynamics based on classical force fields. This method is still expensive to conduct and is currently limited primarily to the study of small inorganic electrolyte systems. Regarding the polymer electrolytes or organic ion conductors such as OIPCs, the use of MD is more prevalent. In recent years, computational studies are increasingly being undertaken and provide significant insights into the study of solid electrolyte systems. [74, 75, 76] Here, we mainly focus on recent progress in computational studies of organic ionic plastic crystals and polymer electrolytes.

4.1. Molecular insights into OIPC simulations

Multiple solid-solid phase transitions are signature thermodynamic phenomena of OIPCs, which are believed to correlate to varied intra and intermolecular ion motions. However. it is a challenge to understand these motions and interactions through experiments alone. On the other hand, this structural evolution can be easily achieved by MD simulations provided that the potential functions are accurate enough to describe molecular structure and motions. With MD simulations, we have successfully reproduced an ion transport model of the OIPC $[P_{122i4}][PF_6]$ that was initially derived from interpretation of the experimental NMR data.[77] Additional specific intra-molecular motions were also captured and presented in greater detail. It is shown that the multiple solid-solid phase transitions are associated with hierarchical thermodynamic ion motions caused by increasing temperature and volume expansion. From the lowest to the highest level, these ion motions could involve (i) the side chain (alkyl chain) vibration and reorientation, (ii) rotation of partial structure or functional groups, (iii) rotation of the whole molecule along a particular direction, (iv) tumbling motion of the whole molecule, and (v) translational or diffusional motion.

Furthermore, it is confirmed that dynamic heterogeneity is present in the OIPC and becomes more pronounced in the presence of molecular defects such as vacancies or grain boundaries. Such a phenomenon was suspected from the NMR linewidth analysis, normally evident as a sharp peak appearing superimposed on a broad static peak (highlighted in **Figure 9**a by a red circle), suggesting a fraction of ions having faster motion than the lattice ions (similar sharp appearing in ^{19}F spectra at 353K, Figure 9b). This was further confirmed through MD simulation of a single $[P_{122i4}][PF_6]$ crystal with Schottky defects (i.e. vacancies introduced in the OIPC by removing ion pairs in the simulation), which promoted ion hopping between nearest neighbor lattice sites,[78] resulting in the collective local fast ion motion.

(Figure 9)

The transport mechanism of the alkali metal ion dopants, including both Li^+ and Na^+, and their impacts on ionic conductivity were also investigated through MD simulations in the $[P_{122i4}][PF_6]$ and tetramethylammonium dicyanamide ([TMA][DCA]) OIPCs.[79, 80] In the [TMA][DCA] system, Li dopants were found to strongly coordinate with the DCA anions, resulting in the shift of the DCA anions from their lattice sites, which increases the free volume in the OIPC, thereby enhancing the diffusion of the remaining "free" DCA anions. This is consistent with experimental observations of the increasing ionic conductivity through adding a small amount of Li salt.[81] The hopping mechanism of both Li^+ and Na^+ inside an OIPC matrix has also been studied in the $[P_{122i4}][PF_6]$,[80] and was found to involve a similar diffusion mechanism to that reported in an ionic liquid electrolyte, in which an alkali metal ion hops through the reconstruction of its first coordination structures. The hopping of the Li^+ in the $[P_{122i4}][PF_6]$ OIPC occurs almost instantaneously as soon as its triangular $Li[PF_6]_3$ solvation structure breaks and reconstructs, whereas the hopping of a sodium ion will go through an intermediate

triangular $Na[PF_6]_3$ solvation structure between the breaking and reconstruction of its tetrahedral $Na[PF_6]_4$ solvation structure, as shown in **Figure 10**. This also explains the slower diffusion of Na^+ compared to Li^+ during the same simulation time.

(Figure 10)

Although some progress has been made towards understanding the thermodynamic properties and ion conduction in OIPC electrolytes, there are still many aspects that remain elusive. For example, it is known that different cation and anion combinations strongly affect the different phase behaviors, plasticity and conductivity in OIPCs. Even for a family of OIPCs with a specific anion or cation, physicochemical properties will be affected significantly by different counterion chemistry.[21] A better understanding of the relationship between ion chemistry, phase behavior and conductivity as well as the effect of substituting different amounts of the OIPC cation with Li^+ cations is required for these solid-state conductors to be further developed. Furthermore, the understanding of how the OIPC interacts with polymers and nanoparticles will certainly benefit the development of OIPC-based composite electrolytes. Computational investigations will surely play a role in this, together with detailed crystallographic and NMR structural and dynamic investigations.

There are still limitations in the computational research of OIPC systems since it requires an initial crystalline structure of an OIPC from experiment, which is not always achievable. The investigation of thermodynamic properties, such as phase transitions, is always done through a heating process, since it is almost impossible to reproduce phase transitions of OIPCs through a simply cooling simulation, without applying extra techniques and methods. Examples of simulating crystallization of ionic liquids into an OIPC can be found from some recent works reported by X. He *et al*. [82] Furthermore,

soft OIPC materials sometimes show the ongoing changes in the crystalline lattice shape at different OIPC phases, which is also a great challenge to accurately reproduce through classical MD simulations. Exploring protonic OIPCs for proton conduction applications needs first-principle based MD simulations that requires even greater computing power in order to cover a wider range of materials, especially those containing large organic cations.

4.2. Simulation-assisted design of advanced polymer electrolytes

The underlying transport mechanisms in polymer electrolytes have also been investigated computationally, by ourselves and others.[69, 76, 77] These studies provide strategies to design the optimal polymer architecture for future research and cover a variety of polyelectrolytes, including both polyanionic and polycationic based systems as well as conventional PEO based polymer systems.[76, 83, 84]

Although the low ionic conductivity hinders the application of anionic polyelectrolytes, its single ion conducting nature still makes this class of materials a favorite research area. One way to tune their ionic conductivities can be achieved through replacing a fraction of the alkali metal ions with a co-cation, e.g. a bulky quaternary ammonium ionic liquid cation, or adding a neutral plasticizer molecule, as demonstrated both experimentally [85] and computationally.[86, 87] MD simulations revealed that the size and amount of the co-cation have a different effect on ionic interactions and transport within the solid electrolyte. In a Li poly(2-acrylamido-2-methyl-1-propanesulfonic acid) (LiPAMPS) system, part of the Li^+ ions were replaced by ammonium cations and the concentration effect of the ammonium was twofold. On one hand, the increased ammonium improved the total ionic conductivity due to the plasticizing effect, and on the other hand it disrupted ion aggregation and thus reduced the ability for Li^+ hopping.

Therefore, an intermediate ammonium concentration of 50 mol% was suggested to maximize Li^+ ion conduction.[87] Furthermore, it was also found that the size of the ammonium cation affects alkali metal ion diffusion; the larger ammonium cations led to more disruption of ion aggregation, and therefore the smaller ammonium cation is a better option to achieve higher conductivity in these systems.[86]

In addition to anionic polyelectrolytes, cationic polyelectrolytes have also been studied recently. As discussed above in the experimental section (section 3.2.2),[69] the behaviors of polymer electrolytes using polyIL as hosts for Li salts are very different from traditional PEO-based polymer electrolytes with respect to T_g and ion dynamics, thus MD simulations have been performed in order to understand these behaviors at a molecular level. In particular, the ion-ion coordination structures were studied and correlated with the transport mechanisms. We proposed a unique co-coordination facilitated transport mechanism in these solid-state conductors (**Figure 11**a). The simulations confirmed that the LiFSI salt plays a dual-role as both the charge carrier and the polymer plasticizer. When increasing amounts of Li salt is dissolved in the polyIL matrix, the overall anion coordination changes from being primarily associated with the polymer backbone to one where the majority of anions bridge between the polymer and the Li^+, which reduces the interaction between polycations and anions, resulting in a reduced T_g.[62] When Li salt is added into the PEO matrix, the polymer chain will immediately solvate the Li^+ by strong PEO oxygen-Li coordination (Figure 11b). This unfavorable polymer-Li^+ coordination crosslinks the system, as evidenced by an increased T_g when a higher concentration of Li salt is used.[63] In contrast to the limited Li^+ transport in PEO-based electrolytes (i.e. the lower diffusion coefficient of Li^+ than FSI, as shown in Figure 11c), a t_{Li+} higher than 0.5 has been achieved in PDADMA FSI-based binary electrolytes due to the faster Li^+ transport relative to the

anion transport (Figure 11d). The MD simulations also suggest that a pair of Li^+ ions can hop in a correlated manner through the bridged FSI anions, thereby enhancing their dynamics and providing another possible mechanism for enhancement of Li diffusion (Figure 11 e-f). Most of these explorations are still in their infancy with rapid progression. There is no doubt that the power of simulation in electrolyte research not only provides a thorough structure-property analysis, but also offers predictive powers that point to new directions in electrolyte research.

(Figure 11)

5. Progress and challenges for prototyping high energy SSLBs

The commonly used cathode materials in current commercial Li-ion battery technologies including LCO, NCA, NMC, LFP have found wide market demand based on their suitability for the performance requirements and operating environments for a given application. While SSLBs can potentially offer several critical improvements in safety and processability over the traditional liquid-based technology, the ability to match the specific energy and power is needed in order to break into the larger markets. The general strategy in this regard is to tailor the SSE properties so that it can facilitate the pairing of a Li metal anode with a cathode material that can operate at high voltages. While there are a number of challenges in tuning the properties of a SSE to facilitate stable and high capacity cycling of a Li metal anode, great progress has been made in this area over the last decade, particularly with the high concentration sulfonylimide-based anion liquid electrolytes (FSI, TFSI, and FTFSI).[40, 88-90] However, less attention has been devoted to overcoming the set of challenges that are present at the high voltage cathode. As a consequence, the most commonly reported cathode material used with SPE materials is LFP (up to 3.8 V vs Li^+/Li) due to the low oxidative stability of most of the reported SPEs. To access the full reversible

capacity of the commercially popular 4 V-class of electrodes such as NCA (4.3 V vs Li^+/Li) and NMC622 (4.5 V vs Li^+/Li), and for attractive non-commercial materials such as LNMO (4.9 V vs Li^+/Li), electrochemical stability at the upper voltage cut-off is required. The challenges here are two-fold, given that there is electrolyte contact with both the active material and the aluminium (Al) current collector, namely (i) the ability to passivate the Al current collector at high potentials (> 4.0 V vs Li^+/Li) to prevent anodic Al dissolution, and (ii) exhibit electrochemical and chemical stability at the active material surface to avoid continuous electrolyte oxidation and impedance buildup. This second point can be addressed by the formation of a kinetically hindering and ionically conducting surface layer, akin to the solid-electrolyte interphase seen at graphitic Li ion battery electrodes. A secondary, but practically significant, feature of a polymer electrolyte is the ability to act as the adhesive and binding agent within the electrode, as has been fulfilled by more conventional binders such PVDF and styrene-butadiene rubber when using a liquid electrolyte to fill the electrode pores and ensure full utilization of the active material.

Highly fluorinated electrolytes based on the FSI and TFSI systems have been widely studied and utilized for their anodic stabilization of Li metal and transport properties that are practical at, or only slightly above, room temperature.[88, 91] The inability of FSI or TFSI to form a passivating layer at the Al current collector continues to limit their application in high voltage cells using conventional solvents. Electrolyte stability at high voltage cathode materials has been shown to depend on various factors such as salt concentration and the coordination environment of the solvent molecules and/or salt ions.[90, 92] As such, ionic liquid and polymer electrolyte systems, in particular those based on the TFSI and FSI anions, have attracted renewed interest as systems in which the Li^+ transport and high voltage stability can be tuned and vastly improved by control of the salt concentration.[93]

5.1. Cathode formulation for high loading battery design

In an effort to evaluate a solid-state electrolyte in isolation from the formulation and design of a solid-state cathode, our early full cell studies were carried out by wetting a traditional PVDF-based porous electrode with an ionic liquid (the same ionic liquid electrolyte that is used as one of the components within the PolyIL).

By imbibing ionic liquids into the cathode to sufficiently fill the pores of a PVDF-based NMC111 cathode, an ionically conducting pathway was introduced into the electrode structure. **Figure 12** shows examples of cells where this approach was employed, using either an OIPC/PVDF nanoparticle composite electrolyte (a & b – an example of a high concentration LiFSI (50 mol% LiFSI/[C_2mpyr][FSI]) OIPC composite with a Li metal | NMC cell) and a polyIL composite electrolyte (c & d – similar to the polyIL electrolytes shown Figure 6 but with additional [C_3mpyr][FSI] IL to enhance electrolyte conductivity). Reasonable stabilities of these electrode materials have been demonstrated, although the contact between polymer and electrode is minimal and thus the high voltage stability of the composite electrolytes is not confirmed up to the high cut-off voltages of 4.5 V that were also tested in this study using an NCA electrode.

(Figure 12)

In practice, the introduction of an additional wetting step into the manufacturing process represents a major barrier towards the feasibility of commercial-scale production. As such, the development of these electrolyte materials must be taken one step further whereby the solid electrolyte material is incorporated into the cathode formulation – ideally as a replacement for the binder – in order to make an all-solid-state cell that can possibly be manufactured using roll-to-roll assembly techniques.

Some of our preliminary (at the time of writing, unpublished) coin cell studies have focused on minimizing the polyIL-based electrolyte content in the electrode slurry

formulation required for a crack-free film morphology. Three electrolyte formulations (20 wt%, 30 wt%, and 40 wt% electrolyte) were cast and SEM images of the resultant films shown in **Figure 13**.

(Figure 13)

Poor film cohesion was observed for 20 wt% and 30 wt% films, while higher contents were smooth and well-adhered to the carbon-coated Al current collectors. The optimum electrolyte content for a crack-free morphology has been determined to be 35 wt% from morphological observations. Li | LFP cells prepared and cycled at 50 °C with a LFP mass loading of 3.6 mg cm^{-2} showed a steady discharge capacity of 0.45 mAh cm^{-2} at C/5. Electrodes with 35 wt % binder were also cast using a 300 μm applicator, however cracking of the electrode was unavoidable despite modifying the drying procedure (under Ar at RT for 48 h, vacuum dried at RT for 48 h, and then vacuum dried at 50 °C for 48 h) to decrease the rate of solvent evaporation.

These results highlight two key issues that are prevalent throughout reported literature on the development of viable solid-state electrolyte materials, (i) underutilization of the active material at practical rates greater than C/20. In most instances, the areal discharge capacities were <80% of the theoretical value calculated from the LFP mass loading, and (ii) achieving towards-practical loading of cathodes of greater than 1 mAh cm^{-2} requires new strategies to avoid intra-film cracking during both drying and cycling, and poor adhesion to the current collector.

Table 1 summarizes some of the recent notable works in the field of solid electrolytes – both polymeric and ceramic – and importantly brings to attention the reported mass loadings and the active material utilization to allow better comparison of the cell study operation parameters and significance. Several strategies have been developed in order to address the two main cathode processing issues of cracking and adhesion. At the top of the materials selection criteria, however, is the need to minimize the interfacial resistance between the cathode ion conductor and the solid electrolyte membrane. The most pragmatic approach for this is to choose the same electrolyte material, or some derivative, in the cathode as in the electrolyte membrane. However, there are some reports where the interface between electrode and electrolyte membrane is mediated by either coating of the electrode active material powder [106, 108, 109]or employing a material that is better suited to fulfilling the role of ion-conductor within the electrode.[110, 112]

Among these works, there are three main cathode fabrication methods that are employed, namely;

(i) adding the electrolyte into the slurry formulation from which the electrode is cast,

(ii) using a conventional PVDF-based cathode which is then imbibed with liquid precursor materials and polymerized *in situ*, and

(iii) a conventional cathode which is then imbibed with a liquid electrolyte.

Comparing the fraction of discharge capacity that is accessed from the total active material, or utilization, shows that neither method provides a clear advantage. However, it has not been shown that method (ii) easily lends itself to fabrication of electrodes with moderate or higher mass loadings. Furthermore, when using methods (ii) and (iii) it is difficult to accurately measure the mass fraction of binder in the electrode structure.

However, given that an additional 5-10 wt% of the electrode is made up of conventional binder, it is reasonable to suggest that the overall active material mass fraction of the total electrode (solid electrode components + ionic conductor) will be lower through these two approaches.

Achieving high areal capacities >1.2 mAh cm^{-2} has, to the knowledge of the authors, not been demonstrated for a SSLB employing a functional binder cast from the electrode slurry with high active material utilization. Indeed, the triblock single-ion conductor developed by Armand in 2013 remains as one of the benchmark systems in this regard with a loading of 0.8 mAh cm^{-2} and a utilization of ~98% at C/15.[45]] As such, the performances achieved here and the testing parameters employed will act as a reliable standard against which to compare.

5.2. High energy SSLB prototyping

Creating a prototype pouch cell which incorporates the features of the plastic crystal or polyIL electrolytes in combination with practical electrode loadings and scale requires all of the factors discussed above to be addressed. Balancing the stability requirements, mechanical properties, ion transport and interfacial properties with the need for scale, processing and low-cost materials creates a challenging materials design problem. In addition, the fabrication and testing of prototype cells presents further complexity where novel approaches and solutions are required to achieve a workable device that not only demonstrates a new electrolyte/electrode formulation but also a step change in cell energy density. Thus, the preparation and testing of new materials in a pouch cell configuration is an essential step towards demonstrating practicality. The prototyping facility at Deakin University's Battery Technology Research and Innovation Hub (BatTRI-Hub) affords the capability to produce up to 14 cm^2 multilayered Li metal

pouch cells that are stacked using a custom-built robotic stacking unit (**Figure 14**a). Our initial efforts at producing single-layered SSLB pouch cells (i.e., three electrodes, cathode|anode|cathode) have achieved stable discharge capacities of 7 mAh (Figures 14b-e). The casting of composite electrodes at high mass loadings (1.5 mAh cm^{-2} and above) while maintaining film cohesion, current collector adhesion, and full active material utilization requires further investigation, both through formulation and testing of novel electrode coatings as well as through further materials design to enhance performance.

(Figure 14)

6. Conclusions and perspectives

The thirst for ever-increasing energy density, coupled with the need for safety, has seen the emergence of all solid-state Li metal batteries as one of the most likely next generation energy storage technologies for applications demanding high performance and safety. Polymers are a truly viable alternative to ceramic or glassy electrolytes, having more desirable mechanical properties with respect to achieving good electrode/electrolyte interfaces and easier fabrication methods. However, the t_{Li+} and overall conductivity still needs to be improved in order for these materials to truly reach their potential. PEO or EO containing polymers are still favored by many researchers, although it has now become evident that these polymers have reached their zenith and new systems must be explored. We have shown several complimentary approaches to design and have implemented new polymer systems with particular emphasis on ionically charged polymer backbones either as hosts for Li salts (with or without additional low molecular weight components such as ionic liquids) or as single-ion conductors in their own right. New polymer chemistries and polymer architectures, as

well as new anion chemistries being developed by Armand, Zhang and coworkers, offer the promise of a step change in ion transport properties in polymer electrolytes. Novel methods of reinforcing the polymer to improve mechanical properties and thermal stability, improve compatibility with the electrodes and move towards solvent free or water-based processing will also be important in enabling a high performance solid-state Li battery technology.

The other promising solid-state conductors, especially when combined with a polymer to form a mechanically strong composite material, are those based on OIPCs. These materials have unique phase dependent transport properties and they are only just beginning to show their promise in recent applications. As with polymers, the chemical design possibilities are vast, and we are exploring these for both Li and sodium ion solid-state conductors. One path currently being pursued is the use of single Li- ion conducting fibers or particles combined with OIPCs to form conducting composites with improved mechanical properties, making use of the interface to dope the OIPC and provide a conductive pathway for Li^+.

The modelling work investigating novel solid electrolytes based on ionic polymer hosts is still at an early stage, but it demonstrates the power to gain new mechanistic understanding. Furthermore, the diversity of chemistry, both with respect to potential ionic polymers as well as the new anions and salts that are being proposed, provides an opportunity for developing new materials. Molecular simulation, without question, will become one of the most proficient tools to explore new chemistries and new strategies to improve the performance of solid-state electrolytes.

To achieve practical all-solid-state and high energy density devices, the design of more electrochemically stable electrolyte systems and improving the cathode assembly

design to incorporate the solid-state ionic conductor are the next steps. Polymer electrolytes based on highly concentrated salt systems have shown their superior stability at elevated voltage. Both polymer electrolytes and OIPCs are good candidates to replace the traditional PVDF binders in the cathodes, given their flexibility and soft characteristics, which will greatly improve the electrode/electrolyte contact. Finally, the structural design and cathode formulation will be another important issue for achieving high energy and sate batteries for practical applications.

Presently there has been substantial focus on so-called glassy and ceramic 'superconductors' due to their record high conductivities (e.g. 2.5×10-2 S cm-1 at 25 ^{o}C for thio-LiSICON electrolyte $Li_{9.54}Si_{1.74}P_{1.44}S_{11.7}Cl_{0.3}$),[114] as well as in the area of high concentration or 'superconcentrated' organic electrolytes,[115] as potential pathways towards better utilisation of the Li metal electrode. However, these 'solid-state' electrolytes have been shown to suffer the same dendrite issues as other systems in spite of their high mechanical modulus along with various interfacial issues which occur during charge-discharge cycling.[12] Likewise, the use of volatile or toxic organic solvents such as ethers and glymes in superconcentrated electrolytes remain to be proven as viable and safe alternatives.[116] Further progress in the development of 'soft' and non-volatile systems such as those described here, addressing issues of chemical/electrochemical stability, dendrite control, efficiency, interfacial contact and interfacial compatibility is urgently needed. Composite systems, bridging traditional domains of polymers, ionic liquids, plastic crystals, ceramics and glasses, along with the use of simulation and chemical design to understand and control ion association and dynamics, provide a diverse range of materials solutions to progress the development of new high energy batteries, including those based the lithium metal anode.

Acknowledgements

This work is supported by the Australia-India Strategic Research Fund (AISRF 48515) and funding from Australian Research Council (ARC) through ARC Centre of Excellence for Electromaterials Science (ACES) program (CE140100012) and Discovery Program (DP140101535). This work is also supported by the Basque Foundation for Science, E-48011 Bilbao, Spain. Dr Nahid Iranipour and Mr Mojtaba Eftekharnia are acknowledged for their assistance with the OIPC and pouch cell testing experimental work.

Received: ((will be filled in by the editorial staff))
Revised: ((will be filled in by the editorial staff))
Published online: ((will be filled in by the editorial staff))

Keywords

organic ionic plastic crystals, polymer electrolytes, high energy density, lithium metal, solid-state lithium batteries

References

[1] a) T. Mandai, K. Dokko, M. Watanabe, The Chemical Record **2019**, 19, 708; b) G. Li, B. Huang, Z. Pan, X. Su, Z. Shao, L. An, Energy & Environmental Science **2019**, 12, 2030; c) J.-Y. Hwang, S.-T. Myung, Y.-K. Sun, Chemical Society Reviews **2017**, 46, 3529.

[2] R. Fang, K. Chen, L. Yin, Z. Sun, F. Li, H.-M. Cheng, Advanced Materials **2019**, 31, 1800863.

[3] C. Liu, Z. G. Neale, G. Cao, Materials Today **2016**, 19, 109.

[4] D. Liu, W. Zhu, J. Trottier, C. Gagnon, F. Barray, A. Guerfi, A. Mauger, H.

Groult, C. M. Julien, J. B. Goodenough, K. Zaghib, RSC Advances **2014**, 4, 154.

[5] Y. Terada, K. Yasaka, F. Nishikawa, T. Konishi, M. Yoshio, I. Nakai, Journal of Solid State Chemistry **2001**, 156, 286.

[6] T. Nagaura, K. J. J. P. Tozawa, Progress in Batteries and Solar Cells **1990**, 9, 209.

[7] L. Suo, O. Borodin, T. Gao, M. Olguin, J. Ho, X. Fan, C. Luo, C. Wang, K. Xu, Science **2015**, 350, 938.

[8] Y. Yung-Fang Yu, J. T. Kummer, Journal of Inorganic and Nuclear Chemistry **1967**, 29, 2453.

[9] W. Luo, Y. Gong, Y. Zhu, Y. Li, Y. Yao, Y. Zhang, K. Fu, G. Pastel, C.-F. Lin, Y. Mo, E. D. Wachsman, L. Hu, Advanced Materials **2017**, 29, 1606042.

[10] a) S. Wenzel, D. A. Weber, T. Leichtweiss, M. R. Busche, J. Sann, J. Janek, Solid State Ionics **2016**, 286, 24; b) S. Wenzel, T. Leichtweiss, D. Krüger, J. Sann, J. Janek, Solid State Ionics **2015**, 278, 98; c) A. Schwöbel, R. Hausbrand, W. Jaegermann, Solid State Ionics **2015**, 273, 51.

[11] a) S. Wenzel, S. Randau, T. Leichtweiß, D. A. Weber, J. Sann, W. G. Zeier, J. Janek, Chemistry of Materials **2016**, 28, 2400; b) N. Kamaya, K. Homma, Y. Yamakawa, M. Hirayama, R. Kanno, M. Yonemura, T. Kamiyama, Y. Kato, S. Hama, K. Kawamoto, A. Mitsui, Nature Materials **2011**, 10, 682.

[12] R. Sudo, Y. Nakata, K. Ishiguro, M. Matsui, A. Hirano, Y. Takeda, O. Yamamoto, N. Imanishi, Solid State Ionics **2014**, 262, 151.

[13] L. Wang, B. Chen, J. Ma, G. Cui, L. Chen, Chemical Society Reviews **2018**, 47, 6505.

[14] https://www.blue-solutions.com/wp-content/uploads/2016/02/BLUE_SOLUTIONS_DR_2015_GB_MEL_22-06-16.pdf.

[15] a) P.-J. Alarco, Y. Abu-Lebdeh, A. Abouimrane, M. Armand, Nature Materials **2004**, 3, 476; b) P. Wang, Q. Dai, S. M. Zakeeruddin, M. Forsyth, D. R. MacFarlane, M. Grätzel, Journal of the American Chemical Society **2004**, 126, 13590.

[16] a) M. Díaz, A. Ortiz, J. M. Pringle, X. Wang, R. Vijayaraghavan, D. R. MacFarlane, M. Forsyth, I. Ortiz, Electrochimica Acta **2017**, 247, 970; b) J. Luo, A. H. Jensen, N. R. Brooks, J. Sniekers, M. Knipper, D. Aili, Q. Li, B. Vanroy, M. Wübbenhorst, F. Yan, L. Van Meervelt, Z. Shao, J. Fang, Z.-H. Luo, D. E. De Vos, K. Binnemans, J. Fransaer, Energy & Environmental Science **2015**, 8, 1276.

[17] a) Q. Li, J. Zhao, B. Sun, B. Lin, L. Qiu, Y. Zhang, X. Chen, J. Lu, F. Yan, Advanced Materials **2012**, 24, 945; b) V. Armel, M. Forsyth, D. R. MacFarlane, J. M. Pringle, Energy & Environmental Science **2011**, 4, 2234.

[18] R. Taniki, K. Matsumoto, T. Nohira, R. Hagiwara, Journal of Power Sources **2014**, 245, 758.

[19] D. R. MacFarlane, M. Forsyth, P. C. Howlett, M. Kar, S. Passerini, J. M. Pringle, H. Ohno, M. Watanabe, F. Yan, W. Zheng, S. Zhang, J. Zhang, Nature Reviews Materials **2016**, 1, 15005.

[20] a) A. Basile, M. Hilder, F. Makhlooghiazad, C. Pozo-Gonzalo, D. R. MacFarlane, P. C. Howlett, M. Forsyth, Advanced Energy Materials **2018**, 8, 1703491; b) H. Zhu, D. R. MacFarlane, J. M. Pringle, M. Forsyth, Trends in Chemistry **2019**, 1, 126.

[21] J. M. Pringle, Physical Chemistry Chemical Physics **2013**, 15, 1339.

[22] J. M. Pringle, P. C. Howlett, D. R. MacFarlane, M. Forsyth, Journal of Materials Chemistry **2010**, 20, 2056.

[23] a) P. C. Howlett, Y. Shekibi, D. R. MacFarlane, M. Forsyth, Advanced Engineering Materials **2009**, 11, 1044; b) P. C. Howlett, J. Sunarso, Y. Shekibi, E. Wasser, L. Jin, D. R. MacFarlane, M. Forsyth, Solid State Ionics **2011**, 204-205, 73; c) J. Sunarso, Y. Shekibi, J. Efthimiadis, L. Jin, J. M. Pringle, A. F. Hollenkamp, D. R. MacFarlane, M. Forsyth, P. C. Howlett, Journal of Solid State Electrochemistry **2012**, 16, 1841.

[24] L. Jin, K. M. Nairn, C. M. Forsyth, A. J. Seeber, D. R. MacFarlane, P. C. Howlett, M. Forsyth, J. M. Pringle, Journal of the American Chemical Society **2012**, 134, 9688.

[25] D. R. MacFarlane, J. Huang, M. Forsyth, Nature **1999**, 402, 792.

[26] N. Iranipour, D. J. Gunzelmann, A. J. Seeber, J. Vongsvivut, A. F. Hollenkamp, M. Forsyth, P. C. Howlett, Journal of Materials Chemistry A **2017**, 5, 24909.

[27] Y. Zhou, X. Wang, H. Zhu, M. Armand, M. Forsyth, G. W. Greene, J. M. Pringle, P. C. Howlett, Physical Chemistry Chemical Physics **2017**, 19, 2225.

[28] Y. Zhou, X. Wang, H. Zhu, M. Yoshizawa-Fujita, Y. Miyachi, M. Armand, M. Forsyth, G. W. Greene, J. M. Pringle, P. C. Howlett, ChemSusChem **2017**, 10, 3135.

[29] L. Jin, P. C. Howlett, J. M. Pringle, J. Janikowski, M. Armand, D. R. MacFarlane, M. Forsyth, Energy & Environmental Science **2014**, 7, 10.

[30] J. Adebahr, N. Ciccosillo, Y. Shekibi, D. R. MacFarlane, A. J. Hill, M. Forsyth, Solid State Ionics **2006**, 177, 827.

[31] Y. Shekibi, A. Gray-Weale, D. R. MacFarlane, A. J. Hill, M. Forsyth, The Journal of Physical Chemistry C **2007**, 111, 11463.

[32] J. M. Pringle, Y. Shekibi, D. R. MacFarlane, M. Forsyth, Electrochimica Acta **2010**, 55, 8847.

[33] Y. Shekibi, S. J. Pas, N. M. Rocher, B. R. Clare, A. J. Hill, D. R. MacFarlane, M. Forsyth, Journal of Materials Chemistry **2009**, 19, 1635.

[34] P. C. Howlett, F. Ponzio, J. Fang, T. Lin, L. Jin, N. Iranipour, J. Efthimiadis, Physical Chemistry Chemical Physics **2013**, 15, 13784.

[35] N. Iranipour, D. J. Gunzelmann, A. Seeber, J. Vongsvivut, C. Doherty, F. Ponzio, L. A. O'Dell, A. F. Hollenkamp, M. Forsyth, P. C. Howlett, Journal of Materials Chemistry A **2015**, 3, 6038.

[36] N. Iranipour, Vol. Doctor of Philosophy, Deakin University, **2016**.

[37] M. Yoshizawa-Fujita, E. Kishi, M. Suematsu, T. Takekawa, M. Rikukawa, **2014**, 43, 1909.

[38] X. Wang, H. Zhu, G. W. Greene, Y. Zhou, M. Yoshizawa-Fujita, Y. Miyachi, M. Armand, M. Forsyth, J. M. Pringle, P. C. Howlett, Advanced Materials Technologies **2017**, 2, 1700046.

[39] Y. Zhou, X. Wang, H. Zhu, M. Armand, M. Forsyth, G. W. Greene, J. M. Pringle, P. C. Howlett, Energy Storage Materials **2018**, 15, 407.

[40] X. Fan, L. Chen, X. Ji, T. Deng, S. Hou, J. Chen, J. Zheng, F. Wang, J. Jiang, K. Xu, C. Wang, Chem **2018**, 4, 174.

[41] L. Long, S. Wang, M. Xiao, Y. Meng, Journal of Materials Chemistry A **2016**, 4, 10038.

[42] M. Armand, J. Chabagno, M. Duclot, "Polymeric solid electrolytes", presented at *Second International Meeting on Solid State Electrolytes, St. Andrews, Scotland*, **1978**.

[43] Z. Xue, D. He, X. Xie, Journal of Materials Chemistry A **2015**, 3, 19218.

[44] J. Mindemark, M. J. Lacey, T. Bowden, D. Brandell, Progress in Polymer Science **2018**, 81, 114.

[45] R. Bouchet, S. Maria, R. Meziane, A. Aboulaich, L. Lienafa, J.-P. Bonnet, T. N. T. Phan, D. Bertin, D. Gigmes, D. Devaux, R. Denoyel, M. Armand, Nature Materials

2013, 12, 452.

[46] J. Chai, Z. Liu, J. Ma, J. Wang, X. Liu, H. Liu, J. Zhang, G. Cui, L. Chen, Advanced Science **2017**, 4, 1600377.

[47] J. Mindemark, B. Sun, E. Törmä, D. Brandell, Journal of Power Sources **2015**, 298, 166.

[48] T. Okumura, S. Nishimura, Solid State Ionics **2014**, 267, 68.

[49] a) L. Meabe, T. V. Huynh, N. Lago, H. Sardon, C. Li, L. A. O'Dell, M. Armand, M. Forsyth, D. Mecerreyes, Electrochimica Acta **2018**, 264, 367; b) L. Meabe, T. V. Huynh, D. Mantione, L. Porcarelli, C. Li, L. A. O'Dell, H. Sardon, M. Armand, M. Forsyth, D. Mecerreyes, Electrochimica Acta **2019**, 302, 414.

[50] a) H. Zhang, C. Li, M. Piszcz, E. Coya, T. Rojo, L. M. Rodriguez-Martinez, M. Armand, Z. Zhou, Chemical Society Reviews **2017**, 46, 797; b) L. Porcarelli, M. A. Aboudzadeh, L. Rubatat, J. R. Nair, A. S. Shaplov, C. Gerbaldi, D. Mecerreyes, Journal of Power Sources **2017**, 364, 191.

[51] L. Meabe, N. Goujon, C. Li, M. Armand, M. Forsyth, D. Mecerreyes, Batteries & Supercaps **2019**, in review.

[52] K. N. Wood, M. Noked, N. P. Dasgupta, ACS Energy Letters **2017**, 2, 664.

[53] L. Suo, Y.-S. Hu, H. Li, M. Armand, L. Chen, Nature Communications **2013**, 4, 1481.

[54] L. Suo, F. Zheng, Y.-S. Hu, L. Chen, Chinese Physics B **2016**, 25, 016101.

[55] H. Yoon, P. C. Howlett, A. S. Best, M. Forsyth, D. R. MacFarlane, **2013**, 160, A1629.

[56] a) A. Ferry, L. Edman, M. Forsyth, D. R. MacFarlane, J. Sun, **1999**, 86, 2346; b) M. Forsyth, D. R. MacFarlane, A. J. Hill, Electrochimica Acta **2000**, 45, 1243; K. Kimura, J. Motomatsu, Y. Tominaga, Journal of Polymer Science Part B: Polymer Physics **2016**, 54, 2442; c) K. Kimura, M. Yajima, Y. Tominaga, Electrochemistry Communications **2016**, 66, 46; d) W. Xu, L.-M. Wang, C. A. Angell, Electrochimica Acta **2003**, 48, 2037.

[57] M. Gouverneur, S. Jeremias, M. Schönhoff, Electrochimica Acta **2015**, 175, 35.

[58] X. Wang, H. Zhu, Gaetan M. A. Girard, R. Yunis, D. R. MacFarlane, D. Mecerreyes, A. J. Bhattacharyya, P. C. Howlett, M. Forsyth, Journal of Materials Chemistry A **2017**, 5, 23844.

[59] X. Wang, G. M. A. Girard, H. Zhu, R. Yunis, D. R. MacFarlane, D. Mecerreyes,

A. J. Bhattacharyya, P. C. Howlett, M. Forsyth, ACS Applied Energy Materials **2019**, accepted.

[60] G. M. A. Girard, X. Wang, R. Yunis, D. R. MacFarlane, A. J. Bhattacharyya, M. Forsyth, P. C. Howlett, Batteries & Supercaps **2019**, 2, 229.

[61] T. M. Pappenfus, W. A. Henderson, B. B. Owens, K. R. Mann, W. H. Smyrl, Journal of The Electrochemical Society **2004**, 151, A209.

[62] X. Wang, F. Chen, G. M. A. Girard, H. Zhu, D. R. MacFarlane, D. Mecerreyes, M. Armand, P. C. Howlett, M. Forsyth, Joule **2019**.

[63] Y. Tominaga, K. Yamazaki, Chemical Communications **2014**, 50, 4448.

[64] M. Watanabe, S. Nagano, K. Sanui, N. Ogata, Solid State Ionics **1988**, 28-30, 911.

[65] H. de Vries, S. Jeong, S. Passerini, RSC Advances **2015**, 5, 13598.

[66] D. G. Mackanic, W. Michaels, M. Lee, D. Feng, J. Lopez, J. Qin, Y. Cui, Z. Bao, Advanced Energy Materials **2018**, 8, 1800703.

[67] N. Goujon, T.-V. Huynh, K. j. Barlow, R. Kerr, K. Vezzù, V. Di Noto, L. A. O'Dell, J. Chiefari, P. C. Howlett, M. Forsyth, Batteries & Supercaps **2019**, 2, 132.

[68] a) M. Forsyth, G. M. A. Girard, A. Basile, M. Hilder, D. R. MacFarlane, F. Chen, P. C. Howlett, Electrochimica Acta **2016**, 220, 609; b) F. Chen, M. Forsyth, Physical Chemistry Chemical Physics **2016,** 18, 19336.

[69] M. Forsyth, L. Porcarelli, X. Wang, N. Goujon, D. Mecerreyes, Accounts of Chemical Research **2019**, 52, 686.

[70] H. Zhang, U. Oteo, H. Zhu, X. Judez, M. Martinez-Ibañez, I. Aldalur, E. Sanchez-Diez, C. Li, J. Carrasco, M. Forsyth, M. Armand, Angewandte Chemie **2019**, 131, 7911.

[71] U. Oteo, M. Martinez-Ibañez, I. Aldalur, E. Sanchez-Diez, J. Carrasco, M. Armand, H. Zhang, ChemElectroChem **2019**, 6, 1019.

[72] M. Armand, M. Gauthier, D. Muller, Google Patents, **1991**.

[73] a) Z. Deng, Y. Mo, S. P. Ong, NPG Asia Materials **2016**, 8, e254; G. Åvall, J. Mindemark, D. Brandell, P. Johansson, Advanced Energy Materials **2018**, 8, 1703036; b) M. D. Bhatt, C. O'Dwyer, Physical Chemistry Chemical Physics **2015**, 17, 4799.

[74] a) P. M. Ketkar, K.-H. Shen, L. M. Hall, T. H. Epps, Molecular Systems Design & Engineering **2019**, 4, 223; b) N. Molinari, J. P. Mailoa, B. Kozinsky, Chemistry of Materials **2018**, 30, 6298.

[75] S. Maheshwari, F. Thakkar, J. Balachandran, S. Sanyal, N. P. Balsara, **2019**, MA2019-03, 256.

[76] S. Mogurampelly, J. R. Keith, V. Ganesan, Journal of the American Chemical Society **2017**, 139, 9511.

[77] F. Chen, L. Jin, S. W. de Leeuw, J. M. Pringle, M. Forsyth, The Journal of Chemical Physics **2013**, 138, 244503.

[78] F. Chen, S. W. de Leeuw, M. Forsyth, The Journal of Physical Chemistry Letters **2013**, 4, 4085.

[79] L. Jin, S. de Leeuw, M. V. Koudriachova, J. M. Pringle, P. C. Howlett, F. Chen, M. Forsyth, Physical Chemistry Chemical Physics **2013**, 15, 19570.

[80] F. Chen, J. M. Pringle, M. Forsyth, Chemistry of Materials **2015**, 27, 2666.

[81] L. Jin, P. Howlett, J. Efthimiadis, M. Kar, D. Macfarlane, M. Forsyth, Journal of Materials Chemistry **2011**, 21, 10171.

[82] a) X. He, Y. Shen, F. R. Hung, E. E. Santiso, The Journal of Chemical Physics **2015**, 143, 124506; b) X. He, Y. Shen, F. R. Hung, E. E. Santiso, The Journal of Chemical Physics **2016**, 145, 211919.

[83] D. J. Brooks, B. V. Merinov, W. A. Goddard, B. Kozinsky, J. Mailoa, Macromolecules **2018**, 51, 8987.

[84] a) Y. Cheng, J. Yang, J.-H. Hung, T. K. Patra, D. S. Simmons, Macromolecules **2018**, 51, 6630; b) J. R. Keith, S. Mogurampelly, F. Aldukhi, B. K. Wheatle, V. Ganesan, Physical Chemistry Chemical Physics **2017**, 19, 29134; c) A. Weyman, M. Bier, C. Holm, J. Smiatek, **2018**, 148, 193824; d) A. Vishnyakov, A. V. Neimark, The Journal of Physical Chemistry B **2000**, 104, 4471.

[85] a) S.-W. Wang, W. Liu, R. H. Colby, Chemistry of Materials **2011**, 23, 1862; G. J. Tudryn, W. Liu, S.-W. Wang, R. H. Colby, Macromolecules **2011**, 44, 3572; b) C. R. Pope, K. Romanenko, D. R. MacFarlane, M. Forsyth, L. A. O'Dell, Electrochimica Acta **2015**, 175, 62; c) Y. V. Oza, D. R. MacFarlane, M. Forsyth, L. A. O'Dell, Physical Chemistry Chemical Physics **2016**, 18, 19011; d) Y. V. Oza, D. R. MacFarlane, M. Forsyth, L. A. O'Dell, Electrochimica Acta **2015**, 175, 80; d) S. A. Mohd Noor, P. C. Howlett, D. R. MacFarlane, M. Forsyth, Electrochimica Acta **2013**, 114, 766.

[86] X. Chen, M. Forsyth, F. Chen, Solid State Ionics **2018**, 316, 47.

[87] X. Chen, F. Chen, E. Jónsson, M. Forsyth, ChemPhysChem **2017**, 18, 230.

[88] J. Qian, W. A. Henderson, W. Xu, P. Bhattacharya, M. Engelhard, O. Borodin, J.-G. Zhang, Nature Communications **2015**, 6, 6362.

[89] Q. Ma, Z. Fang, P. Liu, J. Ma, X. Qi, W. Feng, J. Nie, Y.-S. Hu, H. Li, X. Huang, L. Chen, Z. Zhou, **2016**, 3, 531.

[90] J. Wang, Y. Yamada, K. Sodeyama, C. H. Chiang, Y. Tateyama, A. Yamada, Nature Communications **2016**, 7, 12032.

[91] a) H.-B. Han, S.-S. Zhou, D.-J. Zhang, S.-W. Feng, L.-F. Li, K. Liu, W.-F. Feng, J. Nie, H. Li, X.-J. Huang, M. Armand, Z.-B. Zhou, Journal of Power Sources **2011**, 196, 3623; b) W. Gorecki, M. Jeannin, E. Belorizky, C. Roux, M. Armand, Journal of Physics: Condensed Matter **1995**, 7, 6823; c) S. Lascaud, M. Perrier, A. Vallee, S. Besner, J. Prud'homme, M. Armand, Macromolecules **1994**, 27, 7469.

[92] a) B. Garcia, M. Armand, Journal of Power Sources **2004**, 132, 206; b) J. L. Allen, D. W. McOwen, S. A. Delp, E. T. Fox, J. S. Dickmann, S.-D. Han, Z.-B. Zhou, T. R. Jow, W. A. Henderson, Journal of Power Sources **2013**, 237, 104.

[93] a) Y. Yamada, C. H. Chiang, K. Sodeyama, J. Wang, Y. Tateyama, A. Yamada, ChemElectroChem **2015**, 2, 1687; b) A. S. Best, A. I. Bhatt, A. F. Hollenkamp, Journal of The Electrochemical Society **2010**, 157, A903.

[94] L. Yu, S. Guo, Y. Lu, Y. Li, X. Lan, D. Wu, R. Li, S. Wu, X. Hu, Advanced Energy Materials **2019**, 9, 1900257.

[95] D. Aidoud, D. Guy-Bouyssou, D. Guyomard, J. L. Bideau, B. Lestriez, Journal of The Electrochemical Society **2018**, 165, A3179.

[96] M. Wetjen, G.-T. Kim, M. Joost, G. B. Appetecchi, M. Winter, S. Passerini, Journal of Power Sources **2014**, 246, 846.

[97] H. Ogawa, H. Mori, Polymer **2019**, 178, 121614.

[98] X. Yang, Q. Sun, C. Zhao, X. Gao, K. R. Adair, Y. Liu, J. Luo, X. Lin, J. Liang, H. Huang, L. Zhang, R. Yang, S. Lu, R. Li, X. Sun, Nano Energy **2019**, 61, 567.

[99] I. Aldalur, H. Zhang, M. Piszcz, U. Oteo, L. M. Rodriguez-Martinez, D. Shanmukaraj, T. Rojo, M. Armand, Journal of Power Sources **2017**, 347, 37.

[100] W. Liang, Y. Shao, Y.-M. Chen, Y. Zhu, ACS Applied Energy Materials **2018**, 1, 6064.

[101] Z. Zhu, L.-L. Lu, Y. Yin, J. Shao, B. Shen, H.-B. Yao, ACS Applied Materials & Interfaces **2019**, 11, 16578.

[102] Q. Yu, D. Han, Q. Lu, Y.-B. He, S. Li, Q. Liu, C. Han, F. Kang, B. Li, ACS

Applied Materials & Interfaces **2019**, 11, 9911.

[103] Y.-Y. Sun, Y.-Y. Wang, G.-R. Li, S. Liu, X.-P. Gao, ACS Applied Materials & Interfaces **2019**, 11, 14830.

[104] S. Choudhury, Z. Tu, A. Nijamudheen, M. J. Zachman, S. Stalin, Y. Deng, Q. Zhao, D. Vu, L. F. Kourkoutis, J. L. Mendoza-Cortes, L. A. Archer, Nature Communications **2019**, 10, 3091.

[105] P. Yao, B. Zhu, H. Zhai, X. Liao, Y. Zhu, W. Xu, Q. Cheng, C. Jayyosi, Z. Li, J. Zhu, K. M. Myers, X. Chen, Y. Yang, Nano Letters **2018**, 18, 6113.

[106] L.-P. Wang, X.-D. Zhang, T.-S. Wang, Y.-X. Yin, J.-L. Shi, C.-R. Wang, Y.-G. Guo, Advanced Energy Materials **2018**, 8, 1801528.

[107] S. Hao, H. Zhang, W. Yao, J. Lin, Journal of Power Sources **2018**, 393, 128.

[108] X. Fan, X. Ji, F. Han, J. Yue, J. Chen, L. Chen, T. Deng, J. Jiang, C. Wang, Science Advances **2018**, 4, eaau9245.

[109] W. Zhang, D. A. Weber, H. Weigand, T. Arlt, I. Manke, D. Schröder, R. Koerver, T. Leichtweiss, P. Hartmann, W. G. Zeier, J. Janek, ACS Applied Materials & Interfaces **2017**, 9, 17835.

[110] D. Zhang, L. Zhang, K. Yang, H. Wang, C. Yu, D. Xu, B. Xu, L.-M. Wang, ACS Applied Materials & Interfaces **2017**, 9, 36886.

[111] Q. Guo, Y. Han, H. Wang, S. Xiong, Y. Li, S. Liu, K. Xie, ACS Applied Materials & Interfaces **2017**, 9, 41837.

[112] J. Zhang, N. Zhao, M. Zhang, Y. Li, P. K. Chu, X. Guo, Z. Di, X. Wang, H. Li, Nano Energy **2016**, 28, 447.

[113] D. Lin, W. Liu, Y. Liu, H. R. Lee, P.-C. Hsu, K. Liu, Y. Cui, Nano Letters **2016**, 16, 459.

[114] Z. Zhang, Y. Shao, B. Lotsch, Y.-S. Hu, H. Li, J. Janek, L. F. Nazar, C.-W. Nan, J. Maier, M. Armand, L. Chen, Energy & Environmental Science **2018**, 11, 1945.

[115] Y. Yamada, J. Wang, S. Ko, E. Watanabe, A. Yamada, Nature Energy **2019**, 4, 269.

[116] a) Y. Yamada, M. Yaegashi, T. Abe, A. Yamada, Chemical Communications **2013**, 49, 11194; b) K. Dokko, N. Tachikawa, K. Yamauchi, M. Tsuchiya, A. Yamazaki, E. Takashima, J.-W. Park, K. Ueno, S. Seki, N. Serizawa, M. Watanabe, **2013**, 160, A1304; c) T. M. Pappenfus, W. A. Henderson, B. B. Owens, K. R. Mann, W. H. Smyrl, **2004**, 151, A209.

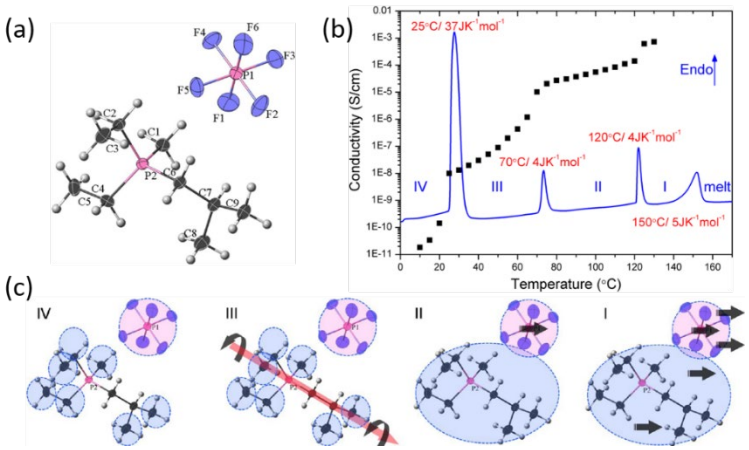

Figure 1. The dependence of ion transport on the solid-solid transitions in a neat OIPC, diethyl(methyl)(isobutyl)phosphonium hexafluorophosphate (P_{122i4}][PF_6]). (a) Structure of one [P_{122i4}][PF_6] ion pair. (b) Solid-solid transitions and ionic conductivity as a function of temperature. (c) The proposed different molecular motions in different solid phases (phase IV to I). Adapted with permission from ref [24]. Copyright 2012 American Chemical Society.

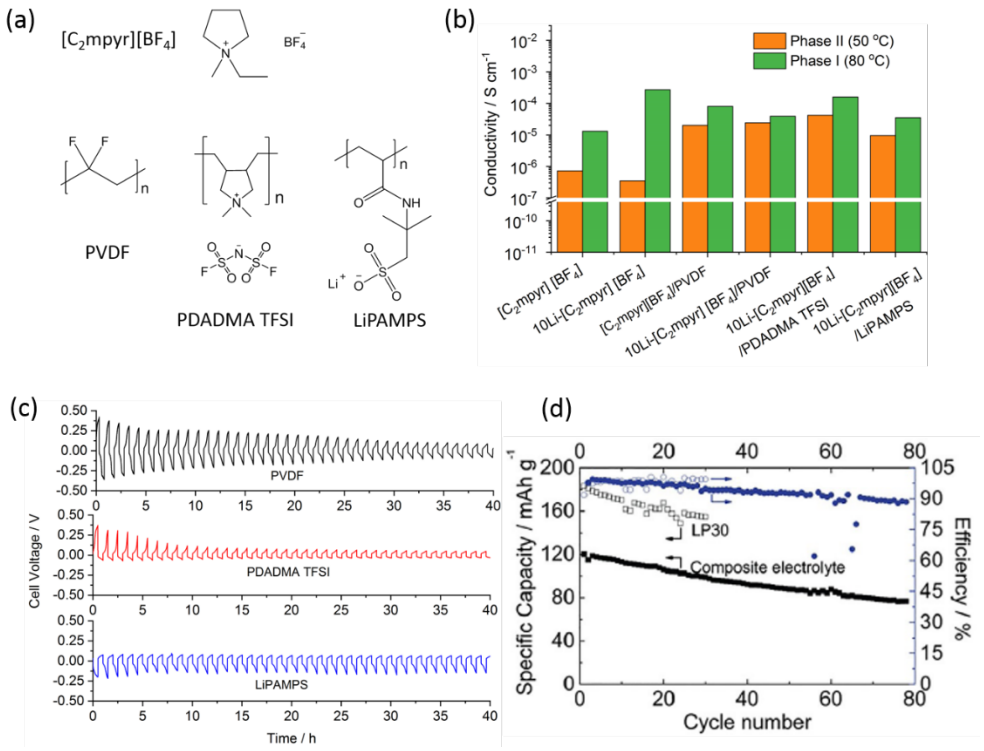

Figure 2. (a) The chemical structures of OIPC [C_2mpyr][BF_4] and polymer fibers used in composite electrolytes. (b) The conductivity comparison of pure [C_2mpyr][BF_4], 10 mol% doped [C_2mpyr][BF_4] (labelled 10Li-[C_2mpyr][BF_4]) and composite electrolytes incorporating different polymer nanofibers. The conductivity data of [C_2mpyr][BF_4], 10Li-[C_2mpyr][BF_4], [C_2mpyr][BF_4]/PVDF and 10Li-[C_2mpyr][BF_4]/PVDF is extracted from ref [35]. The conductivity data of 10Li-[C_2mpyr][BF_4]/LiPAMPS is extracted from ref [36] (c) The cycling performance of the Li | Li symmetric cells assembled with OIPC composites incorporating different nanofibers. (d) discharge performance of a Li | NMC111 cell using 50Li-[C_2mpyr][FSI]/PVDF fiber composite electrolytes (C/15, cut-off voltage 2.5 – 4.6 V, 50 °C). The right-hand side y-axis is columbic efficiency. Reproduced with permission from ref [28]. Copyright 2017 Wiley.

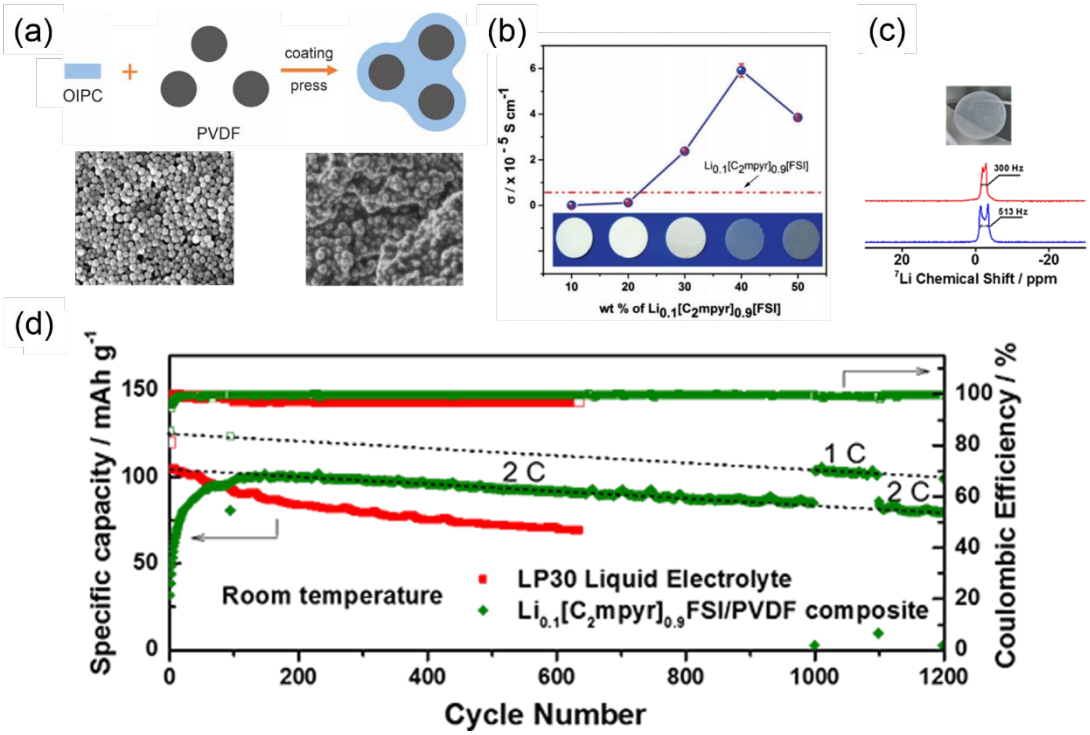

Figure 3. The [C_2mpyr][FSI]-based composite electrolytes using PVDF nanoparticles for Li metal full cells. (a) preparation of OIPC-coated PVDF composites. The SEM images are the PVDF particles before and after OIPC coating. (b) The composition dependence of ionic conductivity of the nanocomposites. (c) ^{7}Li static NMR spectra of 10 mol% LiFSI doped [C_2mpyr][FSI] (bottom, blue) and corresponding composite electrolytes with PVDF particles. (d) discharge performance of Li | LFP cell assembled with composite electrolytes with 10 mol% LiFSI, room temperature. Adapted with permission from ref [38]. Copyright 2017 Wiley

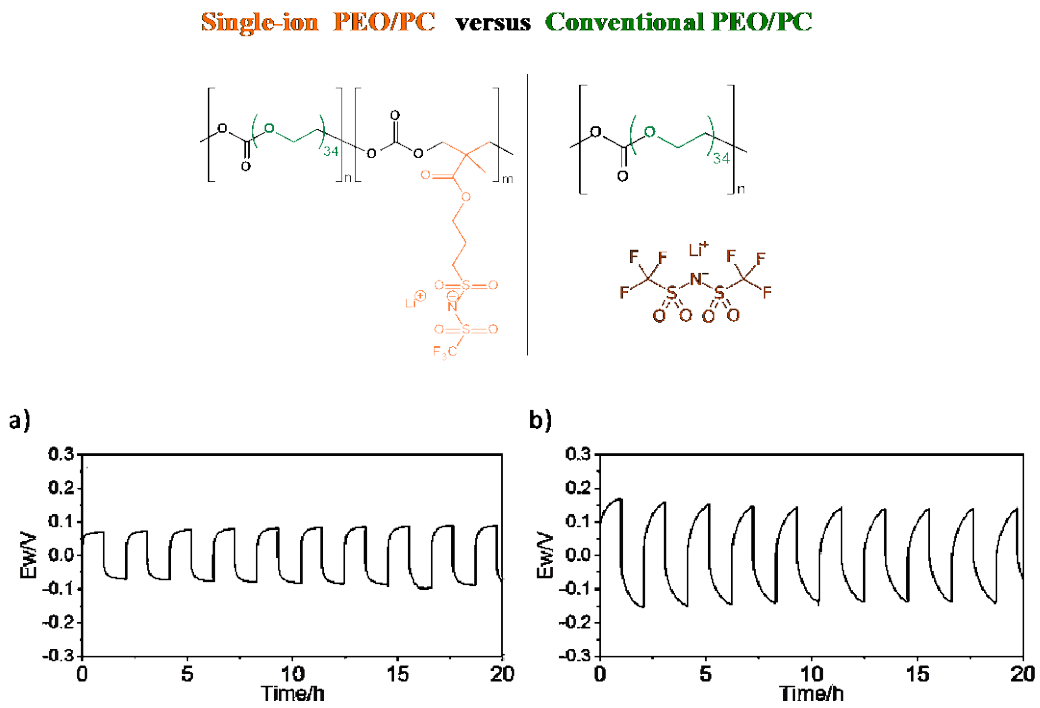

Figure 4. Upper part: Chemical Structures of single-ion PEO/PC and conventional PEO/PC polymer electrolytes. Lower part: Li symmetric cells at 70 °C under 0.2 mA cm^{-2} polarization: a) single-ion PEO/PC and b) Conventional PEO/PC electrolyte with LiTFSI. Data from ref [51].

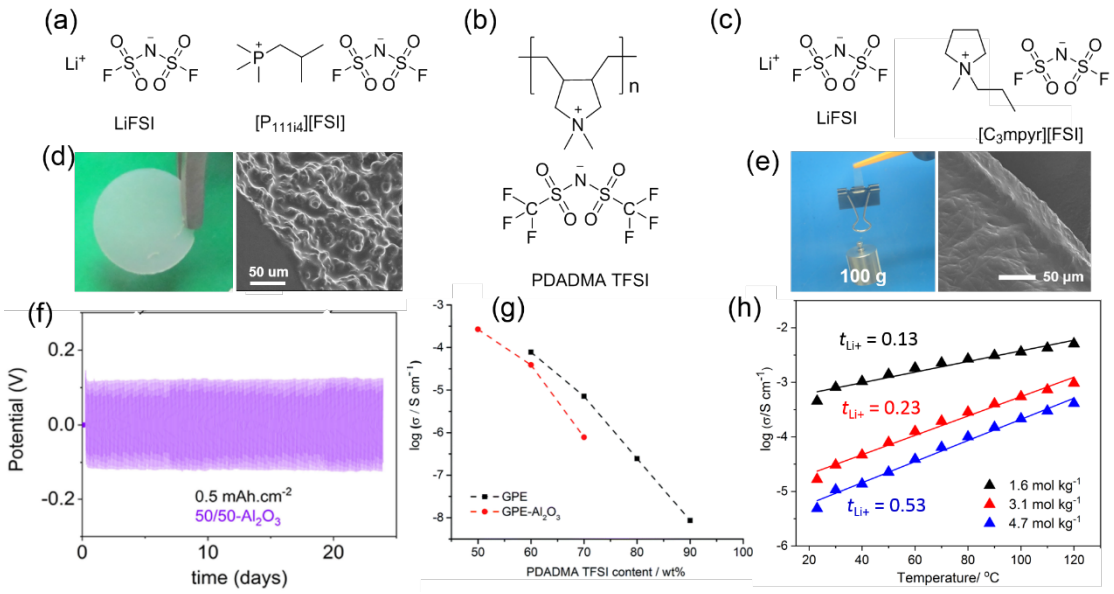

Figure 5. (a)–(c) Chemical structures of LiFSI salt, ionic liquids trimethyl(isobutyl)phosphonium bis(fluorosulfonyl)imide ([P_{111i4}][FSI]), *N*-methyl-*N*-propylpyrrolidinium bis(fluorosulfonyl)imide ([C_3mpyr][FSI]) and PDADMA TFSI host. (d) photograph (left) and SEM image (right) of composite electrolytes consisting high Li concentration [P_{111i4}][FSI] and Al_2O_3 nanoparticles. Adapted with permission from ref [58]. Copyright 2018 The Royal Society of Chemistry. (e) digital picture (left) and cross-sectional SEM image (right) of composite electrolytes consisting high Li concentration [C_3mpyr][FSI] and PVDF nanofibers. Adapted with permission from ref [59]. Copyright 2019 American Chemical Society. (f)-(g) Li | Li symmetric cycling performance and conductivity dependence of composite electrolyte of (d). Adapted with permission from ref [60]. Copyright 2019 Wiley. Reproduced with permission from ref [58]. Copyright 2017 The Royal Society of Chemistry. The salt concertation of 1.6 mol kg^{-1}, 3.1 mol kg^{-1} and 4.7 mol kg^{-1} represents the mole number of salt in one kilogram of "solvent" (ionic liquid plus PDADMA TFSI) in each electrolyte. Reprinted with permission from ref [59]. Copyright 2019 American Chemical Society.

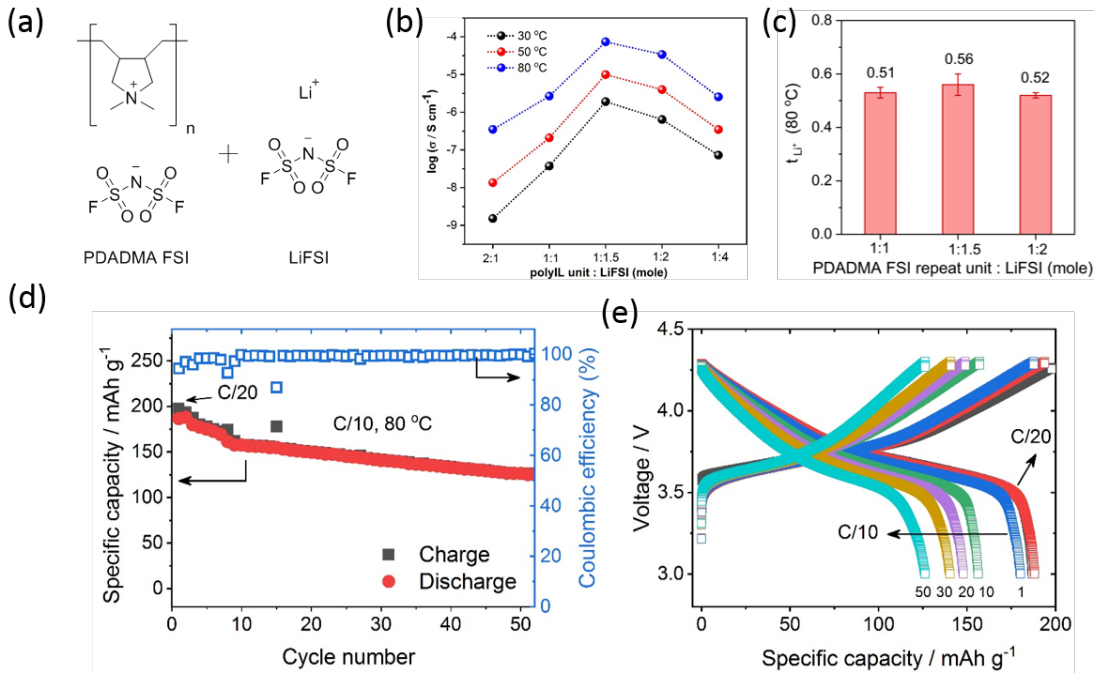

Figure 6. (a) chemical structures of poly(ionic liquid)s, PDADMA FSI and LiFSI salt. (b) conductivity dependence on LiFSI salt concentration. (c) Li^+ transference calculated based on method proposed by Watanabe *et al.*.[64] (d) The cycling performance of Li | NMC cell assembled with PDADMA-LiFSI composite electrolytes. (d) Typical charge-discharge curves corresponding to (d). Adapted with permission from ref [62]. Copyright 2019 Elsevier.

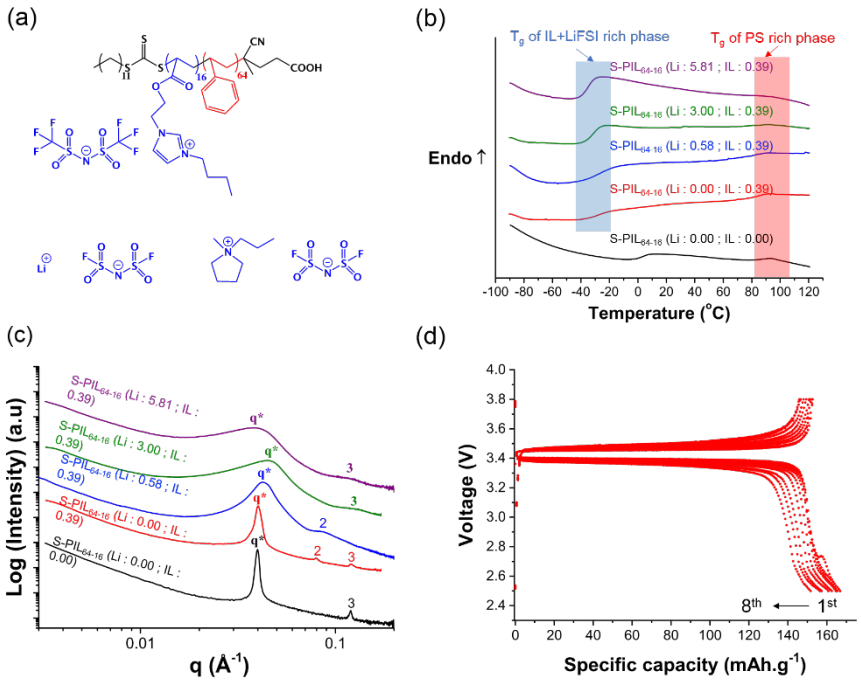

Figure 7. (a) Molecular structure of poly(styrene-*b*-1-((2-acryloyloxy)ethyl)-3-butylimidazolium bis(trifluoromethanesulfonyl)imide) (S-PIL$_{64\text{-}16}$), ionic liquid and Li salt used in this work. (b) Phase behavior and (c) structural relationship of S-PIL$_{64\text{-}16}$ electrolytes as function of IL content and salt concentration. (d) charge-discharge curves of Li | LFP cell at 50 ºC with an areal capacity of 1.8 mAh.cm^{-2} at a C-rate of C/20 using a polyIL block copolymer electrolytes. Reprinted with permission from ref [67]. Copyright 2019 Wiley.

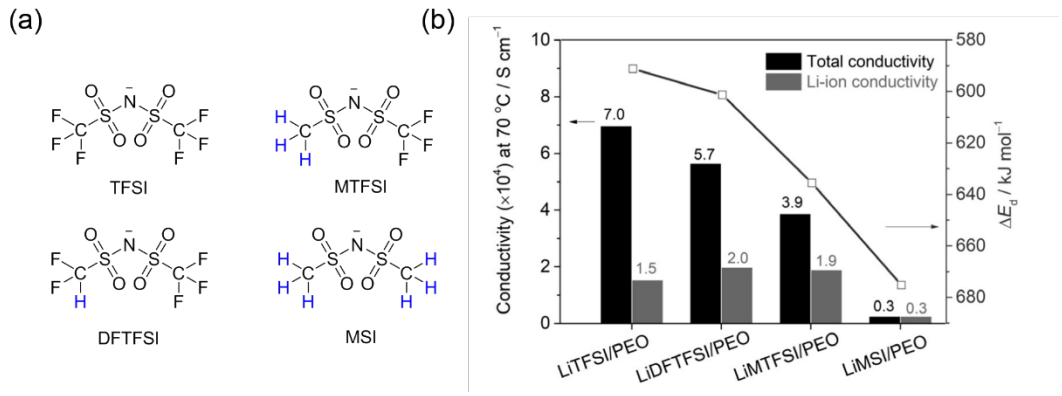

Figure 8. Design of new Li salts for improved Li^+ transport. (a) Anion chemical structures of different Li salts and (b) calculated Li^+ conductivity (70 °C) and dissociation energy of LiX/PEO electrolytes containing different Li salts. Reprinted with permission from ref [70]. Copyright 2019 Wiley

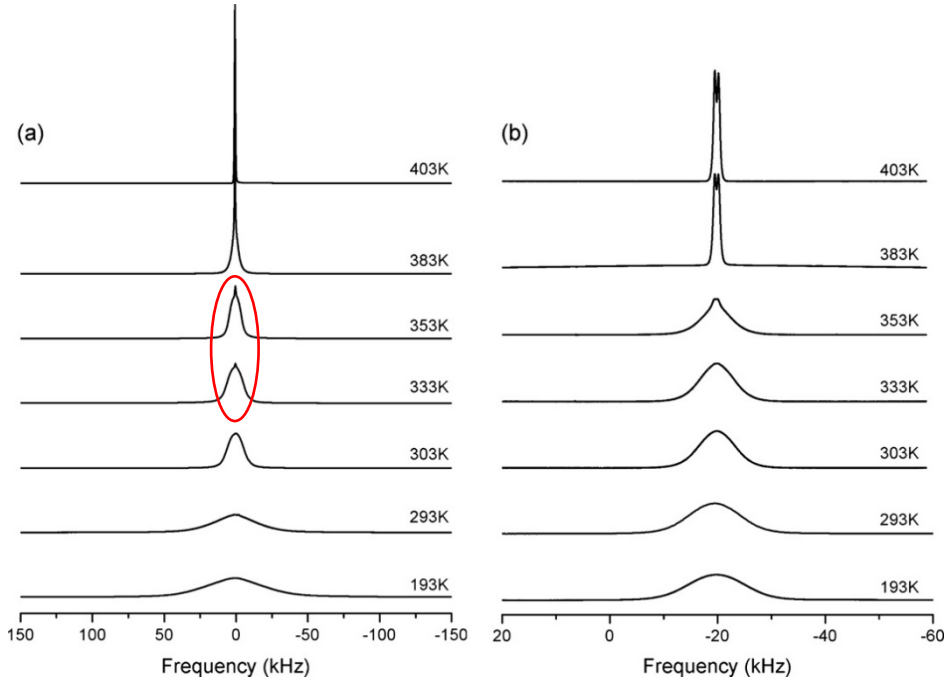

Figure 9. The ^{1}H single-pulse (a) and ^{19}F single-pulse (b) spectra versus temperature for an OIPC $[P_{122i4}][PF_6]$. A sharp peak appears on the top of the broad peak at 333K that is highlighted by the red circle, suggesting a small fraction of fast-moving cations. Adapted with permission from ref [24]. Copyright 2012 American Chemical Society.

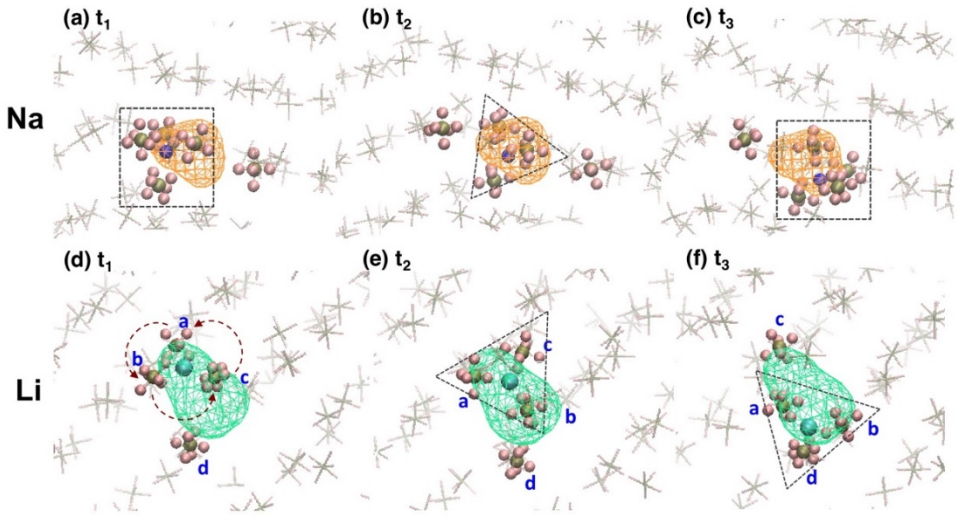

Figure 10. Snapshots of the Na (a)-(c) and Li (d)-(f) doped $[P_{122i4}][PF_6]$ system at three points in time (t_1, t_2, and t_3), demonstrating a hopping process of the metal ion that involves its first solvation shell. The orange and green contours are isosurfaces of the density distribution of Li^+ and Na^+ generated throughout 2 ns, using an isovalue ($\rho_r = \rho(x,y,z)/\rho_{bulk}$) of 0.01. Square/triangular frames are used to highlight the tetrahedral/triangular solvation structures. The highlighted PF_6 anions in the Li-doped system are labeled to illustrate the movements of three PF_6 anions inside the solvation shell. Some of the matrix anions are shown as background to demonstrate the solid plastic crystal phase. Adapted with permission from ref [80]. Copyright 2015 American Chemical Society.

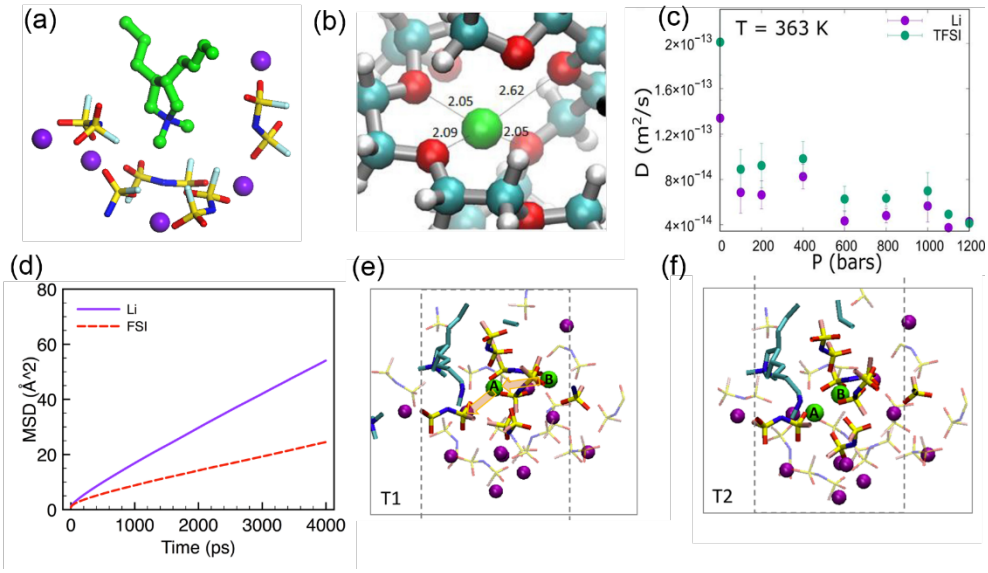

Figure 11. Comparisons of coordination mechanism and ion mobilities between PDADMA FSI-based electrolyte and PEO-based electrolyte by MD simulation. (a) The co-coordination of polycations (green sticks), Li^+ ions (purple balls) and FSI anions (blue, yellow, red and aqua colors are for N, S, O and F atoms) in a PDADMA FSI-LiFSI binary electrolyte. Adapted with permission from ref [62] Copyright 2019 Elsevier. (b) Coordination structure between PEO oxygens (light blue, white and red colors are for C, H and O atoms) and Li^+ (green ball).[83] (c) The diffusion coefficients of Li^+ and TFSI anion in a PEO electrolyte. Adapted with permission from ref [75] (d) Mean square displacement (MSD) of Li^+ and FSI (N atom) in a PDADMA FSI-LiFSI electrolyte at 400 K. Adapted with permission from ref [62] Elsevier. (e-f) snapshots capturing hopping of two adjacent Li^+(A) and Li^+(B) in a PDADMA FSI-LiFSI electrolyte. Adapted with permission from ref [62] Copyright 2019 Elsevier.

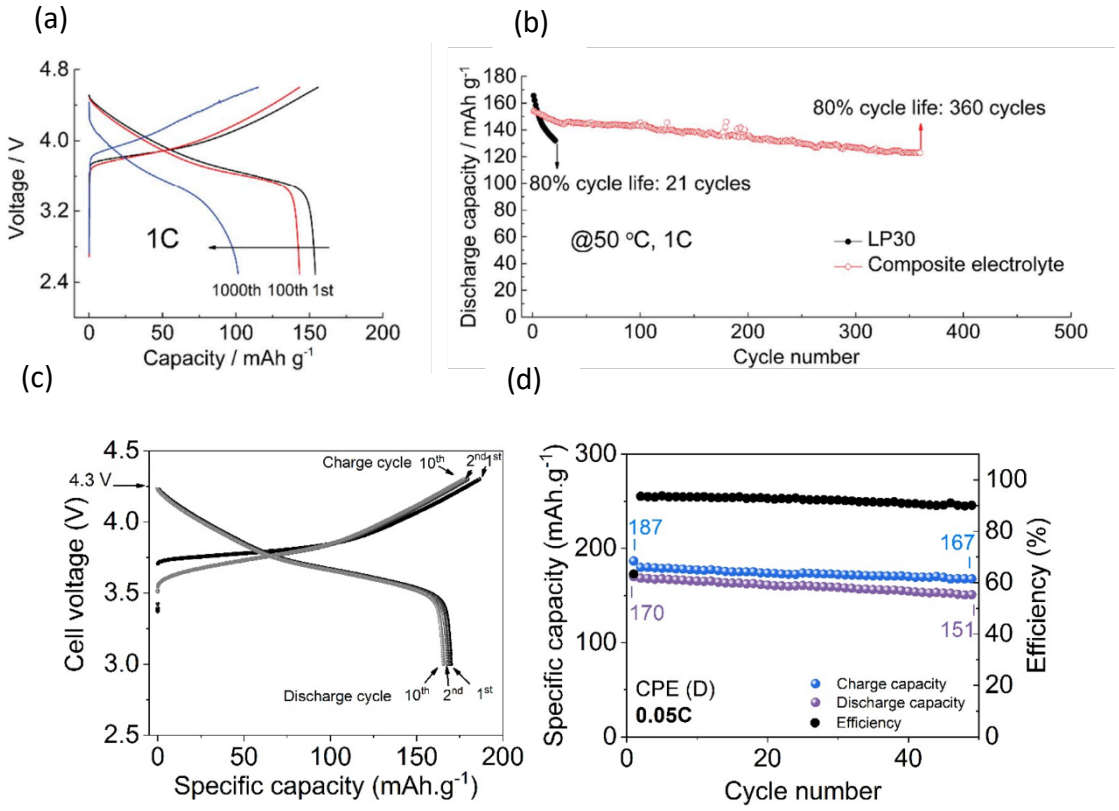

Figure 12. Li | NMC111 cell cycling of the PVDF nanoparticle-based [C_2mpyr][FSI]:LiFSI (1:1 mole fraction) composite electrolytes. (a) the 1st, 100th, and 1000th charge-discharge curves. (b) discharge capacity comparison between LP30 and composite electrolytes for cells cycling at a rate of 1 C at 50 °C. The active material loading of NMC111 is 2.6 mg cm^{-2}. Adapted with permission from ref [39]. Copyright 2018 Elsevier. (c) Charge−discharge profiles after 1, 2, and 10 cycles for Li|NMC111 cells containing PDADMA-TFSI:LiFSI:C_3mpyrFSI (0.18:0.59:0.23 mole fraction) composite electrolyte. (d) Corresponding cycling performance for 50 cycles at 0.05C and 50 °C. The active material loading of NMC111 is 7.2 mg cm^{-2}. Reprinted with permission from ref [59]. Copyright 2019 American Chemical Society.

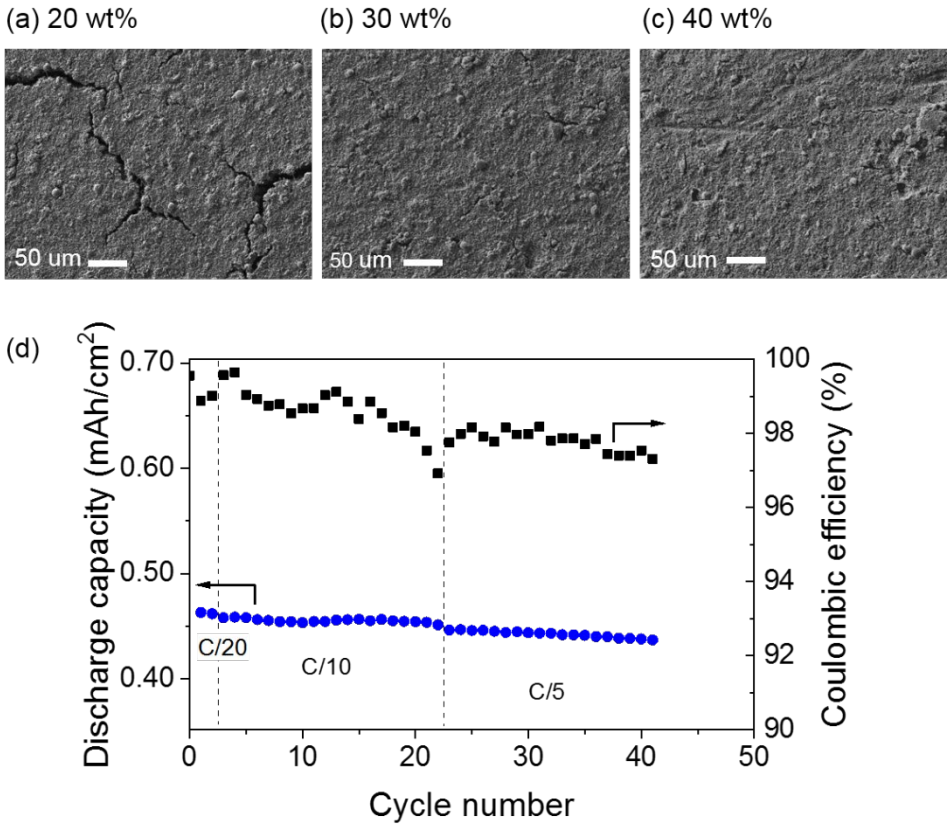

Figure 13. SEM images of an LFP electrode cast using (a) 20 wt%, (b) 30 wt%, and (c) 40 wt% of PDADMA:[C_3mpyr][FSI]:LiFSI binder in the slurry formulation. (d) shows Li | LFP coin cell cycling data for electrodes cast using 35 wt% binder using a 75 µm applicator. The active material loading of LFP was 3.6 mg cm^{-2}.

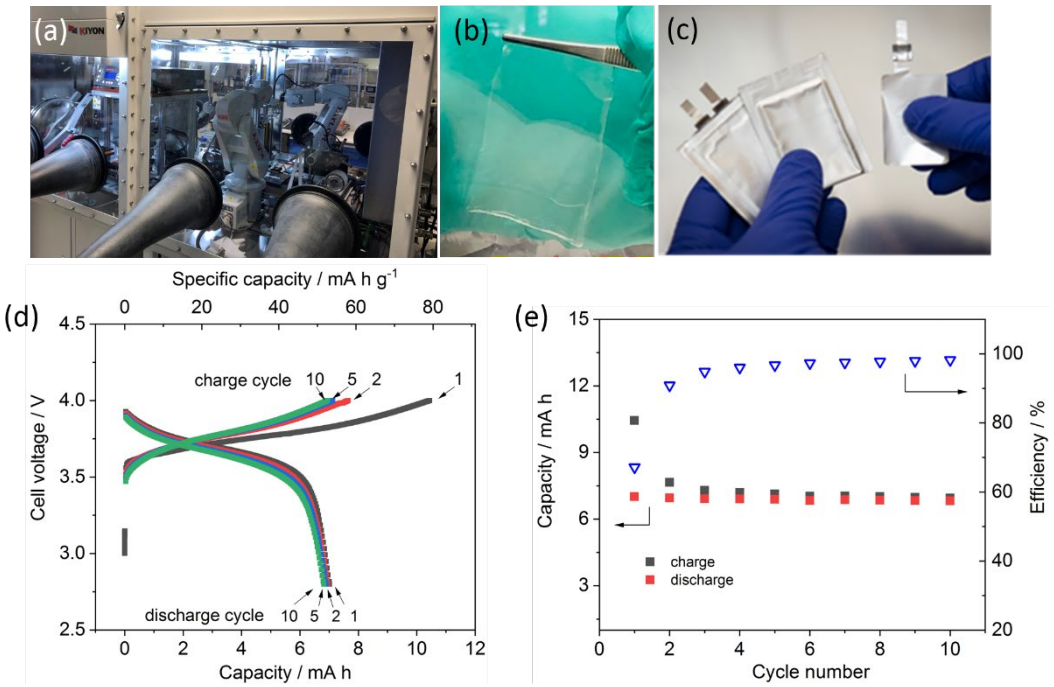

Figure 14. (a) A custom-built robotic stacking unit in Deakin University's Battery Technology Research and Innovation Hub (BatTRI-Hub). (b) PDADMA-TFSI:LiFSI:[C_3mpyr][FSI] composite electrolyte (c) The assembled Li metal pouch cells. The charge/discharge curves (d) and cycling performance (e) of Li | NMC111 pouch cell using PDADMA-TFSI:LiFSI:[C_3mpyr][FSI] composite electrolyte (0.18:0.59:0.23 mole fraction). The pouch cell is cycled at C/20 with a cut-off voltage of 4V, 50 ºC. NMC111 loading is 9.5 mg cm^{-2}.

Table 1. A comparison of the recent reports on SSLBs using different SSEs, binders and electrode materials.

Ref.	Composite cathode preparation method	Electrolyte	Electrolyte in cathode (wt%)	Cathode material	Mass loading (mg cm^{-2})	Theoretical areal discharge capacity (mAh cm^{-2})	Discharge capacity (mAh cm^{-2})	C-rate	T (°C)	Upper cut-off voltage (V vs $Li^+|Li$)
ref[94]	Liquid precursors imbibed	LiTFSI/G4 in DMA-TEOS	10 wt% PVDF	LFP NMC811	1.0 0.8	0.17 0.16	0.14 0.13	C/5 C/10	RT RT	2.5 – 3.9 2.8 – 4.2
ref[95]	Liquid precursors imbibed	[ETPTA/HDDA]/90	8 wt% CMC	LFP	1.0	0.17	0.12	C/20	RT	2.0 – 4.2
ref[96]	Cast from electrode slurry	PEO/LiTFSI/[C_4mpyr][TFSI]	50 wt%	LFP NMC NCA	3.5 4.5 4.5	0.60 0.86 0.72	0.57 0.84 0.71	C/20	40	3.0 – 4.0 3.0 – 4.3 3.0 – 4.3
ref[97]	Liquid precursors imbibed	PDADMA TFSI/ LiTFSI/[C_2mpyr][TFSI]	10 wt% PVDF	NMC111	6.7	1.1	0.5	C/20	50	LTO anode
ref[98]	Cast from electrode slurry and imbibed with solution	PEO/LiTFSI + glass fiber	10 wt%	LFP	10.5	1.79	1.52	C/10	80	2.7 – 4.0
ref[99]	Cast from electrode slurry	Jeffamine/LiTFSI	30 wt%	LFP	5.5	0.94	0.61	C/10	70	2.6 – 3.9
ref[45]	Cast from electrode slurry	P(STFSILi)-*b*-PEO-*b*-P(STFSILi)	32 wt%	LFP	4.7	0.8	0.78	C/15	80	2.5 – 3.8
ref[100]	Liquid precursors imbibed	PEGDA:SN:LiTFSI	Not reported	NCA	Not reported	Not reported	Not reported	C/10	30	2.5 – 4.15
ref[101]	Cast from electrode slurry	PEO/LiTFSI	20 wt%	LFP	2.0	0.34	0.3	1C	60	2.5 – 3.8
ref[102]	Imbibed with LP30	LAGP-3DGPE	10 wt% PVDF	LFP	1.75	0.3	0.28	0.3C	RT	2.4 – 4.2
ref[103]	Liquid electrolyte squeezed from membrane	SA-PHC soaked in LP30	10 wt% PVDF	NCA	7.5	1.5	1.5	1C	55	3.0 – 4.3
ref[104]	Lithion™ solution imbibed	Diglyme-$LiNO_3$-HFiP	PVDF (wt% not reported)	NMC622	10.5	2	1.8	C/5	RT	3.0 – 4.2
ref[105]	Cast from electrode slurry	PVDF/Palygorskite Nanowire Composite	10 wt% PVDF and $LiClO_4$	NMC111	1.6	0.26	0.19	0.3C	RT	3.0 – 4.2

ref[106]	Cast onto active material powder and cast from slurry	Poly(ether-acrylate)	PAB@NMC with 10 wt% PVDF	NMC622 (PAB-coated)	2.0	0.38	0.35	1C	60	2.5 – 4.3
ref[107]	Cast from electrode slurry, and imbibed with liquid electrolyte	LiBr-LLZO	20 wt% LLZO, and 10% PVDF	LCO	1.2	0.33	0.13	C/50	RT	3.2 – 4.2
ref[108]	Cast from electrode slurry	LiFSI-LPS	30 wt% LPS	LCO ($LiNbO_2$ coated)	7.3	1	0.88	C/3	RT	2.6 – 4.2
ref[109]	Cast from electrode slurry	$Li_{10}GeP_2S_{12}$	20 wt% $Li_{10}GeP_2S_{12}$	LCO ($LiNbO_2$ coated)	7.64	1.045	0.91	C/10	RT	2.6 – 4.2
ref[110]	Cast from electrode slurry	PCL/SN/LiTFSI	15 wt% PCL/SN/LiTFSI + 5 wt% PVDF	LFP	1.9	0.32	0.29	C/10	RT	2.5 – 4.2
ref[111]	Cast from electrode slurry	LPELCE	10 wt% PVDF-HFP	LFP	2.2	0.37	0.34	C/20	RT	2.7 – 3.85
ref[46]	Liquid precursors imbibed	PVCA-SPE	10% PVCA	LCO	1.5	0.23	0.22	C/10	50 °C	2.5 – 4.3
ref[112]	Cast from electrode slurry	PEO:LLZTO	10 wt% PVDF:SCN:$LiClO_4$	LFP	9.5	1.6	1.3	C/10	60 °C	2.65 – 3.75
ref[113]	Cast from electrode slurry	SiO_2-PEO	20 wt% PEO-$LiClO_4$	LFP	1.0	0.17	0.15	C/10	90 °C	2.5 – 4.1

Biographies and photographs

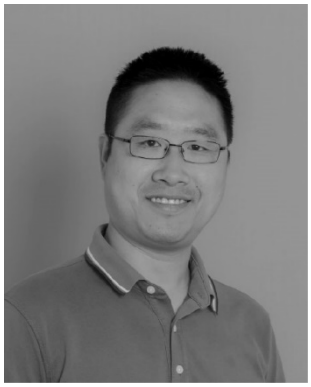

Xiaoen Wang received his PhD in material science in 2011 from Wuhan University of Technology, China. His research interests include solid-state polymer electrolytes, nanocomposites and their applications in energy storage and conversion devices. Currently, he is working with Prof Maria Forsyth as a research fellow and his work is focused on developments of alternative polymer electrolytes and plastic crystal composites for high energy, all-solid-state lithium-, sodium-metal batteries.

Maria Forsyth is an Alfred Deakin Professorial Fellow, an elected Fellow of the Australian Academy of Sciences, Fellow of the Royal Australian Chemical Institute and ISE fellow. She is Associate Director of the ARC Centre of Excellence in Electromaterials Science (ACES), leading the research effort in energy storage and corrosion science at Deakin University in Australia and Director of the Industry Transformation Training Centre, storEnergy. Her work has focused on understanding the phenomenon of charge transport at metal/electrolyte interfaces within novel electrolytes to enable next generation energy devices

Patrick C. Howlett received his Ph.D. from Monash University in collaboration with CSIRO in 2004. His research relates to electrochemical devices and surface engineering through the manipulation of electrode interphases using novel materials approaches. He is currently director of the Battery Technology Research Innovation Hub (BatTRI-Hub) at Deakin University, focused on advanced battery prototyping and translating technologies from lab to industry. His research covers new lithium and sodium battery technologies as well as ionic liquid, polymer and plastic crystal electrolytes and their composites.

Table of contents

High energy density and safe solid-state lithium batteries are vital to advance today's consumer electronics and automobiles applications. This review summarizes the advances in electromaterials research at Deakin University, with focus on alternative solid electrolyte design including organic ionic plastic crystals, novel polymer electrolytes as well as high capacity cathodes.

Keywords

organic ionic plastic crystals, polymer electrolytes, high energy density, lithium metal, solid-state lithium batteries

Xiaoen Wang,* Robert Kerr, Fangfang Chen, Nicolas Goujon, Jennifer M. Pringle, David Mecerreyes, Maria Forsyth, Patrick C. Howlett *

Towards high energy solid-state lithium batteries: opportunities and challenges

ToC figure

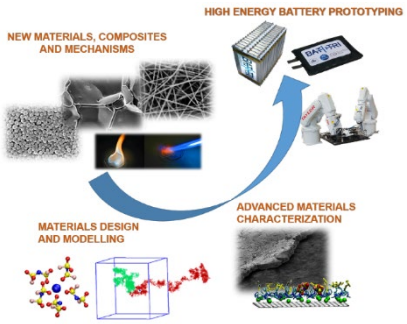

Appendix

SSLBs	Solid-state Li batteries
SSEs	Solid-state electrolytes
SHE	Standard hydrogen electrode
SPE	Solid polymer electrolyte
t_{Li+}	Li^+ transference number
SEI	Solid-electrolyte interphase
LiPON	Lithium phosphorous oxynitride
NASICON	Sodium (Na) Super Ionic CONductor
OIPCs	Organic ionic plastic crystals
DSC	Differential scanning calorimetry
SEM	Scanning electron microscope
NMR	Nuclear magnetic resonance
$[P_{1,2,2,i4}][PF_6]$	Diethyl(methyl)(isobutyl)phosphonium hexafluorophosphate
TFSI	Bis(trifluoromethane sulfonyl)amide anion
FTFSI	Fluorosulfonyl-(trifluoromethanesulfonyl)imide anion
FSI	Bis(fluorosulfonyl)imide anion
$[P_{1i4i4i4}][FSI]$	Triisobutyl methylphosphonium bis(fluorosulfonyl)imide
$[C_2mpyr][TFSI]$	*N*-ethyl-*N*-methyl pyrrolidinium bis(trifluoromethane sulfonyl)amide
$LiBF_4$	Lithium tetrafluoroborate
LiTFSI	Lithium bis(trifluoromethane sulfonyl)amide
LiFSI	Lithium bis(fluorosulfonyl)imide
PVDF	Polyvinylidene difluoride
$[C_2mpyr][BF_4]$	*N*-ethyl-*N*-methyl pyrrolidinium tetrafluoroborate
PDADMA TFSI	Poly(diallyldimethylammonium) bis(trifluoromethanesulfonyl)imide
10Li-$[C_2mpyr][BF_4]$/PDADMA TFSI	A composite electrolyte consisting 10 mol%$LiBF_4$-$[C_2mpyr][BF_4]$ and PDADMA TFSI nanofibers
PolyILs	Poly(ionic liquid)s or polymerized (ionic liquid)s
$[C_2mpyr][FSI]$	*N*-ethyl-*N*-methyl pyrrolidinium bis(fluorosulfonyl)imide
50Li-$[C_2mpyr][FSI]$/PVDF	A composite OIPC electrolyte consisting 50 mol% LiFSI-$[C_2mpyr][FSI]$ and PVDF nanofibers
PEO	Poly(ethylene oxide)
PC	Polycarbonates
PEO/PCs	Poly(ethylene oxide carbonates)
$P_{111i4}FSI$	Trimethyl(isobutyl)phosphonium bis(fluorosulfonyl)imide
$[C_3mpyr)[FSI]$	*N*-methyl-*N*-propylpyrrolidinium bis(fluorosulfonyl)imide
$[C_4mpyr)[TFSI]$	*N*-butyl-*N*-methylpyrrolidinium bis(trifluoromethanesulfonyl)imide
PDADMA FSI	Poly(diallyldimethylammonium) bis(fluorosulfonyl)imide

T_g	Glass transition temperature
RAFT	Reversible addition–fragmentation chain transfer
DCA	Dicyanamide
LiPAMPS	Lithium poly(2-acrylamido-2-methyl-1-propanesulfonic acid) (LiPAMPS)
LP30	A liquid electrolyte consists of 1 mol/L $LiPF_6$ and ethylene carbonate/dimethyl carbonate (EC/DMC) (50/50 wt%)
LFP	Lithium iron phosphate ($LiFePO_4$)
NMCxyz	Lithium nickel cobalt manganese oxide ($LiNi_xMn_yCo_zO_2$)
NCA	Lithium nickel cobalt aluminum oxide ($LiNiCoAlO_2$)
LCO	Lithium cobalt oxide ($LiCoO_2$)
LNMO	Lithium nickel manganese spinel ($LiNi_{0.5}Mn_{1.5}O_4$)
G4	Tetraglyme
TEOS	Tetraethoxysilane
DMA	*N, N′* - dimethylacrylamide
ETPTA	Trimethylolpropane ethoxylate triacrylate
HDDA	*1,6*-hexanediol diacrylat
CMC	Carboxymethyl cellulose
DADMA	Diallyldimethyl ammonium
STFSI	Styrene trifluoromethanesulphonylimide
PEGDA	Poly(ethylene glycol) diacrylate
SN	Succinonitrile
LAGP	$Li_{1.5}Al_{0.5}Ge_{1.5}(PO_4)_3$
3DGPE	Three-dimensional gel polymer electrolyte
SA-PHC	Sodium alginate-poly(vinylidene fluoride-*co*-hexafluoropropylene)-cellulose acetate
HFiP	Tris(hexafluoro-iso-propyl)phosphate
PAB	Poly(acrylonitrile-*co*-butadiene)
LLZO	$Li_{6.25}La_3Zr_2Al_{0.25}O_{12}$
LPS	Li_3PS_4
PCL	Poly(ε-caprolactone)
LPELCE	LAGP−P(VDF-HFP)−ethylmethylimidazolium TFSI−LiTFSI
PVDF-HFP	Poly(vinylidene fluoride-*co*-hexafluoropropylene)
PVCA	Poly(vinyl carbonate)
LLZTO	$Li_{6.4}La_3Zr_{1.4}Ta_{0.6}O_{12}$